From tryptophan to novel mitochondria-disruptive agent, synthesis and biological evaluation of 1,2,3,6-tetrasubstituted carbazoles

Milena Witkowska[a]‡, Natalia Maciejewska[b]‡, Małgorzata Ryczkowska[a], Mateusz Olszewski[b], Maciej Bagiński[b], Sławomir Makowiec[a*]

[a]Department of Organic Chemistry, Faculty of Chemistry, Gdansk University of Technology, Narutowicza 11/12, 80-233, Gdansk, Poland.
[b]Department of Pharmaceutical Technology and Biochemistry, Faculty of Chemistry, Gdansk University of Technology, Narutowicza 11/12, 80-233, Gdansk, Poland.
‡These authors contributed equally.

Abstract: Mitochondrial targeting plays an important role in anticancer therapy. The Mn(III)-promoted cyclization of 5-(1H-indol-3-yl)-3-oxopentanoic acid allow to obtain novel substituted carbazole derivatives that can act as mitochondria-disruptive agents. The starting materials used for the synthesis of these new aminocarbazoles are oxopentanoate derivatives of tryptophan. The scope and limitation of this method of synthesis are determined by a series of experiments. The prepared carbazole derivatives are screened for their *in vitro* anticancer activity against a broad panel of human cancer cells and normal cell lines. Among the tested compounds, the most active ones are examined further against human colon cancer cells (HCT-116) and human bone osteosarcoma (U-2 OS), in complex *in vitro* cellular assays, including studies on cell cycle distribution, intracellular compartmentalization, antimigratory properties, mitochondrial generation of reactive oxygen species, DNA damage, and type of cellular death. The results reveal that the synthesized compounds display potent oxidative activity inducing massive accumulation of DNA double-strand breaks, which lead to a parallel change in the assembly of mitochondria causing their dysfunction. These findings provide new leads for the treatment of colon cancer and osteosarcoma.

1. Introduction

For over half a century, the carbazole scaffolds have been a predominant structural motif of many biologically active compounds used in medicine, including both natural and synthetic molecules. The carbazole motif can be found in drugs including alkaloids,[1,2] HIV-integrase inhibitors, [3] antipapillomavirus agent, [4] α- and β-adrenoreceptor antagonists, [5,6] antinausea drug ondasteron, [7] antitumor agents, [8,9] and antimicrobial agents. [10] However, to ensure a wide application of carbazole derivatives, there is a need to develop efficient methods of synthesis. A significant number of synthesis methods have been proposed for these derivatives so far. Among them, we can specify the synthetic routes based on the reaction of biaryls. These routes include the use of a biphenyl moiety bearing a nitrogen atom in ortho position which reacts mostly by oxidative cyclization pathway to produce a carbazole structure with PhI(OAc)$_2$ as an oxidizer, [11,12] cyclization of biphenyl ortho-substituted triazene moiety, [13] reductive cyclization of o-nitrobiaryls, [14] and double N-arylation of 2,2′-biphenylene ditriflate (**Scheme 1**). [15] Another group of the proposed approaches makes use of an indole fragment and results in the formation of a third aromatic ring. These include gold-catalyzed cyclization of 3-acylindole/ynes, [16] reaction of indole-ynones with nitromethanes, [17] Pd/Cu-cocatalyzed cross-coupling of 2-allyl-3-iodoindoles with terminal alkynes, [18] and synthesis of carbazoles from indoles, ketones, or alkenes using oxygen as an oxidant. [19]

The third group of approaches for the synthesis of carbazole derivatives involves the use of two separate phenyl systems as starting materials. These include oxidative ring fusion using hypervalent iodine compounds [20] and palladium-catalyzed N-arylation followed by oxidative biaryl coupling. [21]
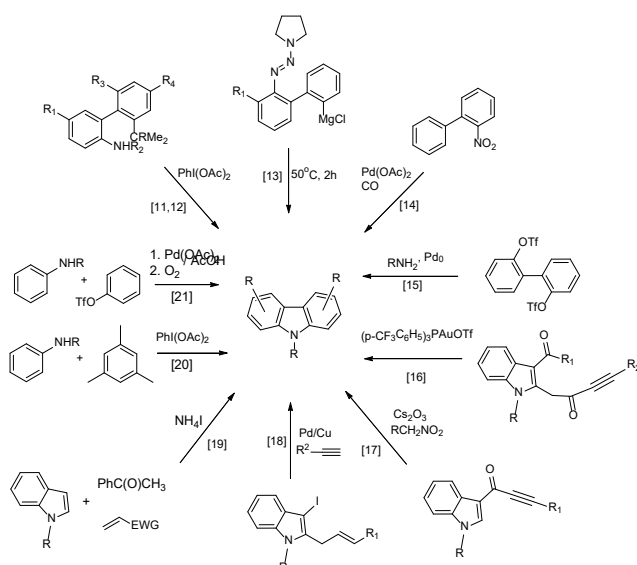
Scheme 1. Selected examples of the synthesis routes of carbazole scaffold.

Recently, we developed a method for the formation of functionalized carbazoles using indole derivatives as starting materials. In this method, 5-(1H-indol-yl)-3-oxo-pentanoate undergoes oxidative cyclization and aromatization with a manganese triacetate or $NEt_3/I_2/Ln(OTf)_3$ system. [22] However, we focused on designing and synthesizing a carbazole core with improved anticancer properties. According to previous *in silico* studies, a carbazole scaffold functionalized with one or two amino groups at positions 3 and 6 can show enhanced anticancer potency if it is acylated or alkylated. [23,24]

A combination of these two ideas—developing a new method for the preparation of functionalized carbazole scaffold and improving its pharmacological properties—prompted us to investigate if it is possible to obtain a carbazole scaffold with amino groups at positions 3 and 6 through oxidative cyclization of 5-(1H-indol-yl)-3-oxo-pentanoates and subsequently subject the prepared carbazoles to acylation or alkylation (**Figure 1**). Although a number of carbazole derivatives with anticancer potential have been discovered in the past two decades, the phenomenon of chemoresistance of tumors urges us to search for novel molecules with anticancer properties. Therefore, in this work, we synthesized a series of new 3,6-substituted carbazole derivatives and examined their antiproliferative activity, in order to develop potent antitumor agents.
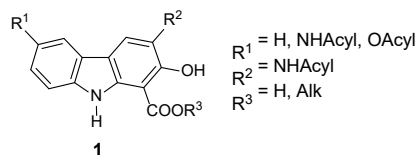
Figure 1. Structures of the newly designed carbazoles.
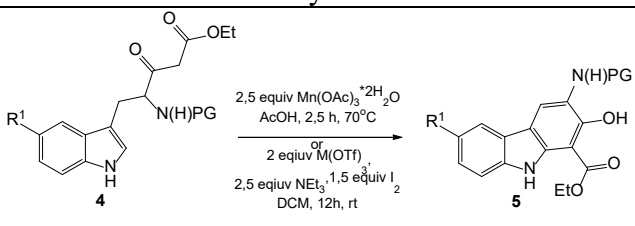
2. Results and discusion

2.1. Chemistry

As described in our previous work, for undergoing oxidative cyclization with an Mn(OAc)$_3$ or NEt$_3$/I$_2$/Ln(OTf)$_3$ system, the substrate must contain indole and 3-oxopentane fragments. Thus, tryptophan was used as a substrate as it contains an amine group at position 3. The availability of substrates plays an important role in the selection of such an approach. A wide range of tryptophan derivatives, which are the substrate at the first stage of synthesis, are available. However, in the light of oxidizing conditions during the cyclization reaction, the presence of an amino group can lead to undesirable side reactions. In addition, for introducing two amino/amido/hydroxy groups, the tryptophan derivative used for cyclization must be functionalized with an amino, amido, or hydroxyl group at position 6. The synthetic strategy used for the preparation of compounds based on 1,2,3,6-tetrasubstituted carbazole scaffold is depicted in **Scheme 2**.
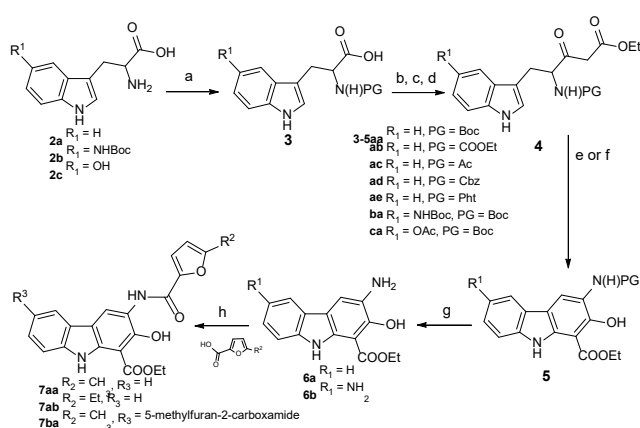
Scheme 2. Reagents and conditions used for the preparation of compounds based on 1,2,3,6-tetrasubstituded carbazoles scaffold: (a) PA, 190°C, 15' or Ac$_2$O, MeOH, 12 h or Boc$_2$O, NaHCO$_3$, dioxane, 24 h or Cbz-Cl, K$_2$CO$_3$, Acetone; H$_2$O; (b) CDI, THF, 2 h, 20°C (c) MgCl$_2$, KOOCCH$_2$COOEt, 1 h, 20°C, (d) 50°C, 12 h; (e) Mn(OAc)$_3$*2 H$_2$O 2.5 eq, AcOH, 2.5 h, 70°C (f) M(OTf)$_3$ 2 eq, NEt$_3$ 2.5 eq, I$_2$ 1.5 eq, DCM, 12h, 20°C; (g) Only in the case of PG or R^1 = NHBoc, TFA, DCM, 2h, 20°C; (h) TBTU, NEt$_3$, DMF

Tryptophans **2** were protected in a typical manner with five different protective groups: permanent Pht, [25] Ac, [26] etoxycarbonyl, [27] and two easily removable Z[28] and Boc. [29] In the next step, a tryptophan derivative was activated with carbonyldiimidazole followed by the carbon acylation of potassium enolate, resulting in the formation of ketoesters **4**. [30,31] Based on our previous experience with oxidative cyclization of 3-oxoesters and 3-oxoamides[22] at the key stage of synthesis, we decided to investigate two available methods. The first one involved the generation of 1,3-dicarbonyl radicals using manganese triacetate followed by cyclization and subsequent oxidation and aromatization. [32–35] The second method was applied for ring closure using a combination of transition metal triflates together with iodine in the presence of a tertiary amine. The results obtained for the cyclization of ketoesters **4** are presented in **Table 1**.

Table 1. Results of oxidative cyclization of ketoesters **4**.

| Entry	4, 5	MX_3	R^1	PG	Yield of **5** [%]
1	aa	$Y(OTf)_3$	H	Boc	12
2	aa	$Sc(OTf)_3$	H	Boc	-
3	aa	$Mn(OAc)_3$	H	Boc	67
4	ab	$Mn(OAc)_3$	H	COOEt	28
5	ac	$Mn(OAc)_3$	H	Ac	29
6	ad	$Mn(OAc)_3$	H	Cbz	-
7	ae	$Y(OTf)_3$	H	Pht	-
8	ae	$Sc(OTf)_3$	H	Pht	-
9	ae	$Mn(OAc)_3$	H	Pht	-
10	ba	$Mn(OAc)_3$	NHBoc	Boc	36
11	ca	$Mn(OAc)_3$	OAc	Boc	25

The experiments clearly demonstrated that application of manganese triacetate is advantageous for the cyclization of ketoesters. Ytrium triflate showed low effectiveness,

whereas scandium triflate did not show any benefits in the cyclization of ethyl 3-((tert-butoxycarbonyl)amino)-2-hydroxy-9H-carbazole-1-carboxylate. These results are in line with our previous observations which also proved that Mn(OAc)$_3$ was effective for the cyclization of ketoesters while transition metal triflates with iodine should be used for the cyclization of ketoamides.[22]

It was observed that the phthaloyl-protected derivative did not undergo oxidative cyclization regardless of the applied oxidation system. This finding is surprising considering that this derivative was believed to be the least susceptible to side reactions when in contact with an oxidizing reagent. We also did not obtain the desired product with Cbz-protected derivative; however, in this case, we expected a negative result due to the possible oxidation and radical reactions of benzyl protons.

Molecular docking performed in studies on anticancer agents[23] indicated that an effective structure should contain a second acyloamino or acyloxy group at position 6 of the carbazole system. Therefore, we attempted to prepare compounds **5ba** and **5ca**. In addition, molecular docking studies indicated the need for a five-member aromatic ring with one or two amino groups as a substituent. Thus, in the next step, we removed the acid-labile amino protective group and performed acylation with 2-furoic acid or 5-methyl-2-furoic acid under typical conditions. The results of the synthesis of furanoyl derivatives are summarized in **Table 2**.

Table 2. Synthesis of ethyl 3-(5-alkylfuran-2-carboxamido)-2-hydroxy-9H-carbazole-1-carboxylate derivatives **7aa-ba**.
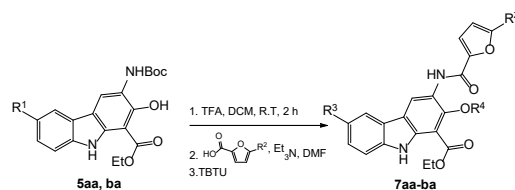
Run	**5**	R^1	R^2	R^3	R^4	**7**	Yield of **7** [%]
1	aa	H	CH$_3$	H	H	aa	15
2	aa	H	Et	H	H	ab	31
3	ba	NHBoc	CH$_3$	(structure)	(structure)	ba	54

To increase water solubility and bioavailability, the most promising compound **5aa** was saponified to obtain 3-((tert-butoxycarbonyl)amino)-2-hydroxy-9H-carbazole-1-carboxylic acid **8** (**Scheme 3**).
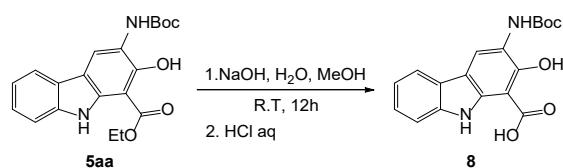

Scheme 3. Saponification of ester **5aa**.

2.2. Biological activity

2.2.1. Effects of carbazole derivatives on the viability of the panel of human cell lines

The newly synthesized carbazole derivatives were screened for their in vitro anticancer activity against a broad panel of human cancer cell lines, including human non-small cell lung adenocarcinoma (A-549), human colon cancer (HCT-116), human bone osteosarcoma (U-2 OS), human breast carcinoma (MCF-7), human liver cancer cells (Hep-G2), and normal human embryonic kidney cells (HEK293) using the colorimetric MTT (3-(4,5-dimethylthiazol-2-yl)-2,5-diphenyltetrazolium bromide) assay. We found that most of the compounds were inactive at IC$_{50}$>50 µM (half maximal inhibitory concentration or IC$_{50}$ refers to the concentration of a compound required to inhibit cell growth by 50% compared to the untreated control), while others exhibited a moderate (**9**, **5ca**) or remarkable (**5aa**, **8**) activity toward the tested cell lines (**Table 3**). Among the cancer cell lines used for the analysis, **5aa** and **8** showed potent antiproliferation activity at submicromolar concentrations against HCT-116 and U-2 OS cells after 72 h of treatment (**Figure 2** and **Table 3**).
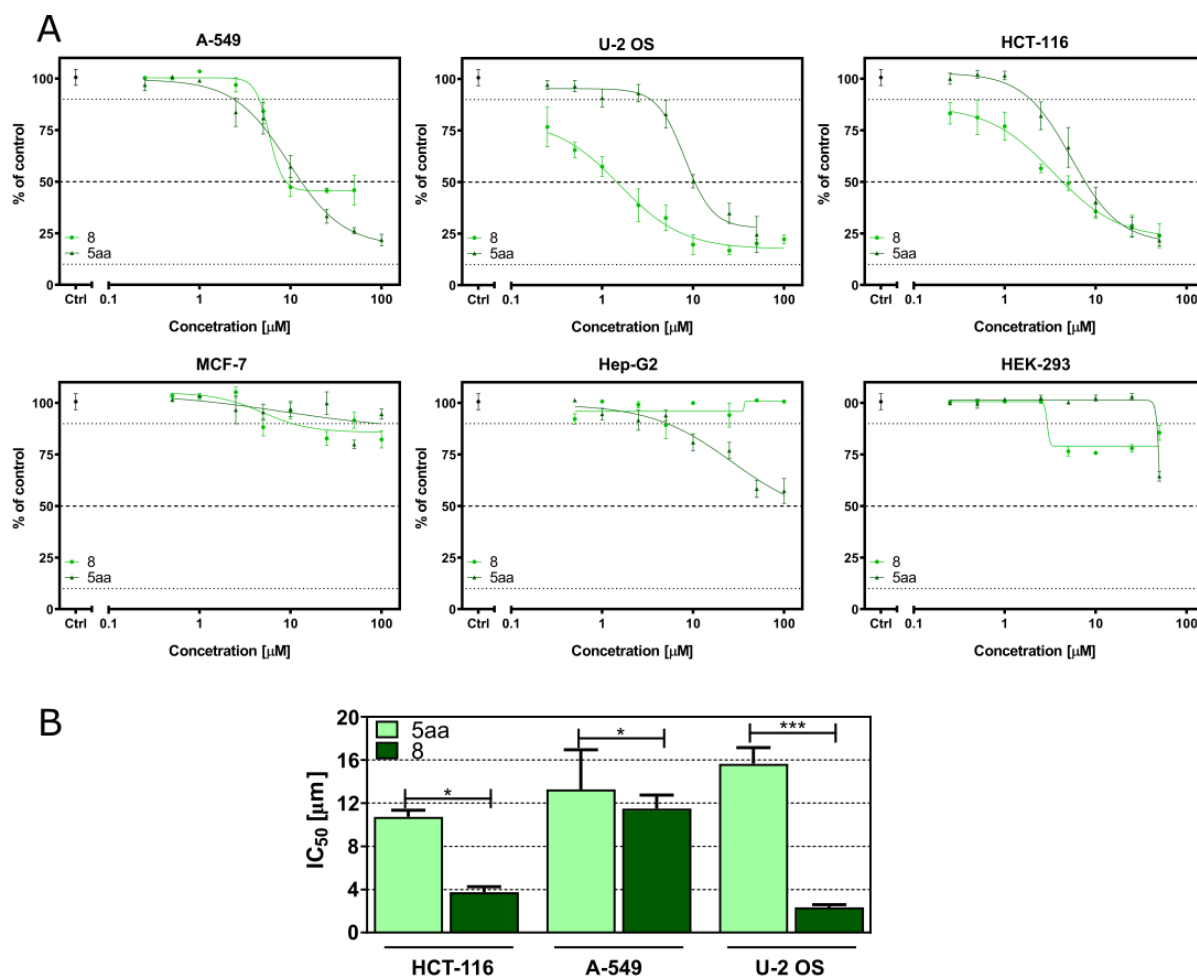
Figure 2 Effects of the carbazole derivatives on the viability of A-549, U-2 OS, HCT-116, Hep-G2, MCF-7, and HEK-293 cells after treatment for 72 h. (**A**) Dose–response curves of **5aa** and **8** were determined by the MTT assay. (**B**) IC$_{50}$ values estimated for compounds **5aa** and **8**. All data are presented as mean±SD of n=3 independent experiments performed in triplicates. Statistical differences were analyzed with a one-way ANOVA post hoc Bonferroni test. *$p< 0.01$, ***$p<0.0001$ vs. vehicle.

Table 3 *In vitro* anticancer activity of carbazole derivatives (IC$_{50}$±SD (µM)) on A-549, HCT-116, U-2 OS, MCF-7, Hep-G2, and HEK-293 cell lines.

| Compound	Cell Lines					
	HCT-116	A-549	MCF-7	U-2 OS	Hep-G2	HEK-293
	IC$_{50}$ [µM]					
9[22]	28.82 ±1.432	>50	>50	43.17±2.07	>50	>50
4aa	>50	>50	>50	>50	>50	>50
5aa	10.73 ±0.61	16.94 ±0.75	>50	15.65±1.50	>50	>50
5ab	>50	>50	>50	>50	>50	>50
5ac	>50	>50	>50	>50	>50	>50
5ba	>50	>50	>50	>50	>50	>50
5ca	46.43 ±3.25	>50	>50	37.50±2.13	>50	>50
7aa	>50	>50	>50	>50	>50	>50
7ab	>50	>50	>50	>50	>50	>50
7ba	>50	>50	>50	>50	>50	>50
8	3.75 ±0.49	11.50 ±1.23	>50	2.35 ±0.24	>50	>50
5-FU	5.78±0.38	8.12± 1.01	8.41± 0.98	13.02±0.03	18.98± 1.98	41± 0.87

Compared to **5aa**, compound **8** showed a significant 3–6 times higher cytotoxic potency. **(Figure 2)** The IC$_{50}$ of compound **8** determined for HCT-116 and U-2 OS cells was 3.75±0.49 and 2.35±0.24 µM, respectively (**Table 3**). Although, none of the tested compounds displayed toxicity against the human noncarcinogenic HEK-293 cell line. Further studies were carried out only on the most cytotoxic compounds **5aa** and **8** to compare the changes in their biological activity depending on their structure. In addition, the compounds were tested for antimicrobial activity. The obtained results indicated that the compounds did not show any activity against the tested strains of bacteria and fungi, which proves their selectivity toward cancer cells (**Table S1**, Supporting Information).

2.2.2. Effects of new carbazole derivatives on cell cycle distribution

To investigate whether the high cytotoxic activity of the newly synthesized compounds (**5aa**, **8**) was caused by the cell cycle arrest, we analyzed the DNA content of cells by flow

cytometry. The stained DNA histograms of A-549, HTC-116, and U-2 OS cells treated with each of the derivatives at the IC_{50} values for 24, 48, and 72 h are shown in **Figure 3**. For HCT-116 cell line, the highest number of cells were observed in the G2/M phase, a moderate number in the S phase, and the least number in the G0/G1 phase after 24 h of treatment with compound **8**. Similar results were observed for all cell lines after 24 h of treatment with this compound. In HCT-116 cell line, continuous treatment with **8** induced the S phase arrest which lasted for 72 h. However, in A-549 cell line, cell cycle progression through the G2/M phase peaked between 24 and 48 h, and the cells were finally arrested in the S phase after 72 h of incubation.
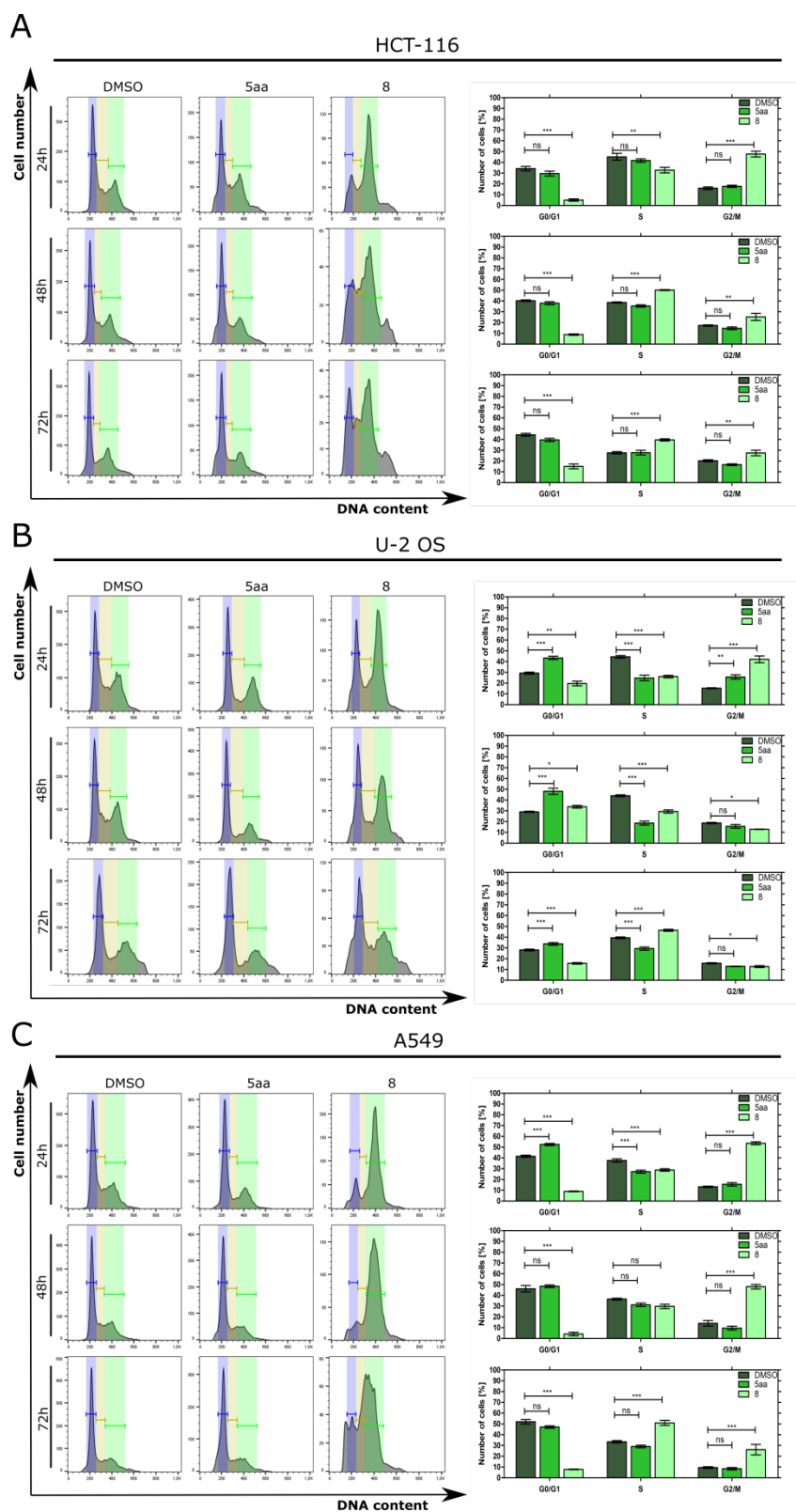
Figure 3 Cell cycle analysis of HCT-116 (**A**), U-2 OS (**B**), and A-549 (**C**) cells after treatment with compounds **5aa** and **8**. The left panel shows representative histograms obtained after DNA staining. The right panel represents the results of statistical analyses of histograms. Error bars represent the SEM of data obtained in n=3 independent experiments. Statistical differences were analyzed with a one-way ANOVA post hoc Bonferroni test. *$p<0.01$, **$p<0.001$, ***$p<0.0001$ vs. vehicle.

Colony formation assays were performed to measure the clonogenic survival of HCT-116 and U-2 OS cell lines which were the most susceptible to the tested compounds. The results showed that both compounds **5aa** and **8** significantly decreased the colony-forming ability of cell lines compared to the control group (1% dimethyl sulfoxide (DMSO) alone), and the effect was more pronounced with increasing doses (**Figure 4A** and **Figure 4B**). Compound **8** caused a greater decrease in clonogenicity in U-2 OS (**Figure 4C**) and HCT-116 (**Figure 4D**) cell lines (75.5% (1 µM) and 84.5% (10 µM), respectively), compared to **5aa**.
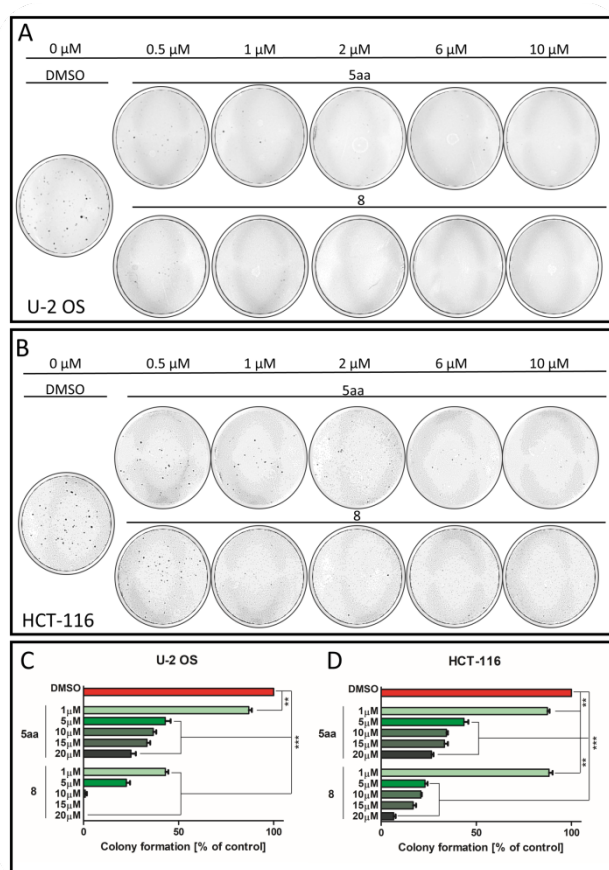
Figure 4 Colony-forming ability of U-2 OS (**A**) and HCT-116 (**B**) cell lines after treatment with control (DMSO) and tested compounds (**5aa**, **8**). Quantitative clonogenicity assays are illustrated in (**C**) and (**D**). Error bars represent the SEM of data obtained in n=3 independent experiments. **$p<0.001$, ***$p<0.0001$ vs. vehicle.

### 2.2.3. Selective accumulation of *5aa* and *8* in cancer cell LDs revealed by intrinsic fluorescence

The inherent fluorescence of compounds allowed determining their fate in living cells by high-resolution laser scanning confocal microscopy. The local fluorescence of both compounds suggested their compartmentalization to a specific intracellular organelle, and thus their accumulation in adiposomes. The cell distribution of the tested compounds was evaluated after short-term exposure and after co-labeling with the neutral lipid dye BODIPY. In the HCT-116 cell line, after 2 h of treatment, localization of **8** and **5aa** was clearly visible, with considerable accumulation in lipid droplets (LDs) (**Figures 5A–C** and **Figures S1A–C**). To evaluate whether the signal of the compounds spatially overlapped with that of BODIPY, correlations of overlapping pixel intensities were calculated using thresholded Mander's (MCC) and Pearson's colocalization coefficient (PCC) (**Figure 5F** and **Figure S1F**, Supporting Information). The results showed high correlation coefficients for both **5aa** (MCC: 0.922±0.055; PCC: 0.723±0.046) and **8** (MCC: 0.935±0.067; PCC: 0.811±0.056), indicating the substantial colocalization between compounds- and BODIPY-derived signals. This proves that **5aa** and **8** selectively accumulated in the LDs of the treated cells. Representative line scan (corresponding to the top panel in **Figure 5A**) showing the colocalization of LDs with compounds is presented in **Figure 5D** and **Figure S1D**. Scatter plots showing the correlations of compound/BODYPI pixel intensities are depicted in **Figure 5E** and **Figure S1E**. The mechanism of accumulation of compounds in adiposomes is unknown, but it can be assumed that the high hydrophobic character of those molecules favored their selective partitioning into an oil-like hydrophobic environment inside LDs. Recent reports suggest that the efficacy of drugs can be modulated by LDs, which constitute their store and supplement the enzymes necessary for the metabolism of hydrophobic small molecules, influencing their activation.[36]
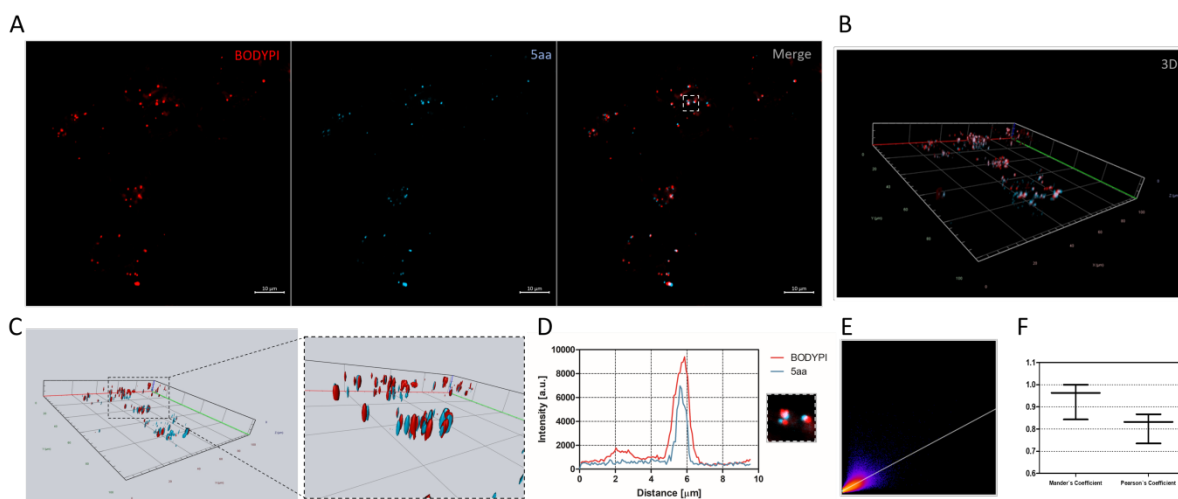
Figure 5 Colocalization analyses. (**A–C**) Representative confocal images showing the intracellular colocalization of LDs (BODYPI) with compound **5aa** in HCT-116 cell line captured in Z-stack (**B**) and rendered with three-dimensional reconstruction (**C**). (**D**) Representative line scan (corresponding to top panel in (**A**)) showing the colocalization of LDs with compounds. (**E**) Scatter plot corresponding to the colocalization of pixels. (**F**) Correlations of overlapping pixel intensities are described as thresholded MCC and PCC from Z-stack images.

2.2.4. Antimigratory properties

One of the first steps of cancer metastasis is cell migration, which is a hallmark of malignancy. Therefore, we studied the antimigratory effect of carbazole derivatives on HCT-116 and U-2 OS cell lines using a wound healing assay. In comparison to solvent-treated cells, treatment with compounds **8** and **5aa** caused dose-dependent inhibition of migration in both cells, which was tracked by time-lapse microscopy (**Figure 6A** and **Figure 6B**). After 24 h of exposure to the tested compounds, the inhibition of migration in HCT-116 cell line was not found to be significant. However, treatment with 10 μM of each compound caused significant inhibition of migration after 60 h ($56.97\pm9.64\%$ and $64.37\pm6.181\%$ by **5aa** and **8**, respectively) (**Figure 6C**). The antimigratory property of **5aa** was less pronounced in U-2 OS cells, but compound **8** showed a greater antimigratory activity in these cells in comparison to HCT-116 cells (**Figure 6C** and **Figure 6D**). Interestingly, the migration-inhibitory effect of **8** was higher in both cell lines and at any point in time of treatment in comparison to **5aa**.
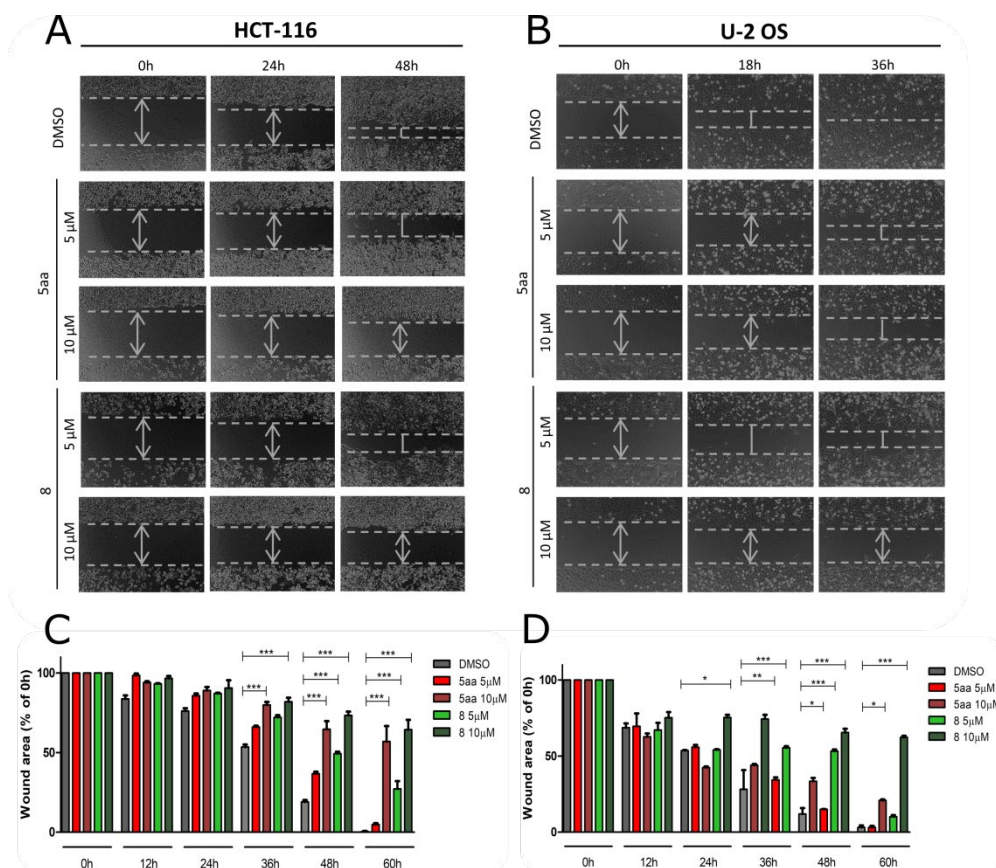
Figure 6 Analysis of cell migration by *in vitro* wound healing assay. Time-lapse microscopy images of wound closure of untreated and compound **5aa** and compound **8**-treated HCT-116 (**A**) and U-2 OS (**B**) cell lines at 0, 24, and 48 h after the removal of culture insert. Scale bars=100 μm. Quantification of wound area is shown in (**C**) and (**D**). Data represent the mean±SEM of n=3 independent experiments. Statistical differences were analyzed with a one-way ANOVA post hoc Bonferroni test. $^{ns}p>0.05$, $***p<0.0001$ vs. vehicle.
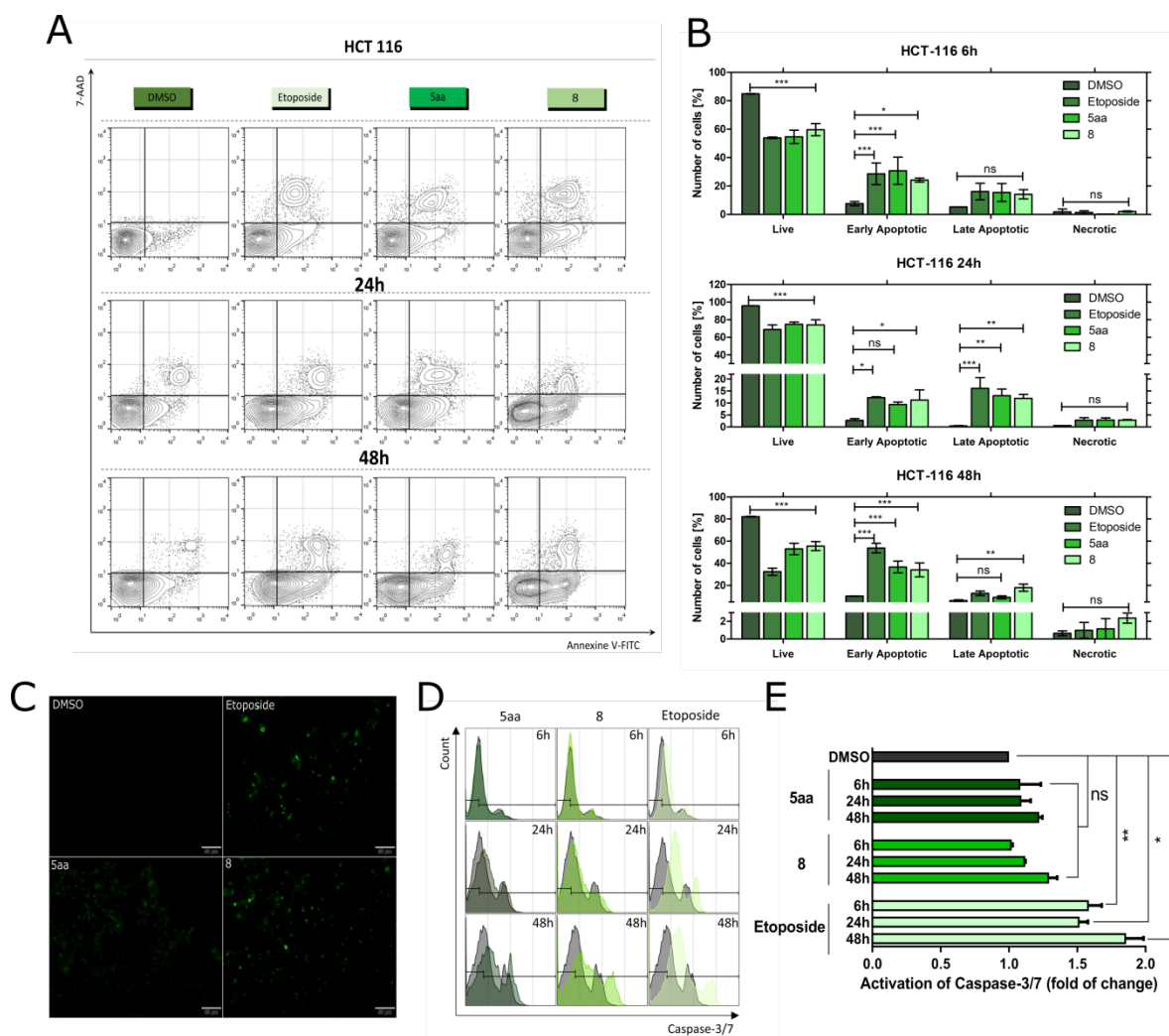
2.2.5. Apoptosis

To further assure the proapoptotic activity of compounds **5aa** and **8**, a flow cytometric analysis was performed, after dual-staining the cells with 7-aminoactinomycin D (7-AAD) and Annexin V-fluorescein isothiocyanate (FITC) which allows differentiating the viable, early apoptotic, late apoptotic, and necrotic cells. After 6 h of treatment with compound **5aa** and **8** at their IC_{50} concentration, a significant decrease in the percentage of surviving cells was observed for HCT-116 cell line (**Figure 7A** and **Figure 7B**). An increase in the percentage of early apoptotic cells was observed with both compounds, but only in the case of cells treated with **8** the increase was significant (11.23±2.97%; $p<0.01$). As shown in **Figure 7A** and **Figure 7B**, after 24 h of exposure to both compounds, a threefold augmentation in apoptosis (early and late) was observed in treated cells in comparison to vehicle. Further

incubation (48 h) caused a significant increase in the percentages of apoptotic cells, while necrotic fraction was determined at 1.16±0.83% and 2.38±0.41% after treatment with **5aa** and **8** compounds, respectively (**Figure 7A–C**). These results confirmed that **5aa** and **8** can trigger apoptotic rather than necrotic cell death in HCT-116 cell line. Interestingly, in the U-2 OS cell line, no apoptosis was observed at any of the studied time points (**Figure S2**, Supplementary Information).

Caspases are crucial cell mediators of programmed cell death related to the stages of apoptosis.[37] Therefore, we investigated the effect of compounds **5aa** and **8** on the activation of two effector caspases: caspase-3 and caspase-7. Both these caspases play an important role in cell apoptosis. In the HCT-116 cell line, both compounds caused a negligible change in the activation of caspase-3/7 in comparison to DMSO (**Figure 7D** and **Figure 7E**). This suggests that apoptosis of cells proceeded through a caspase-independent death effector pathway.

Figure 7 Apoptosis assay. (**A**, **B**) Flow cytometric analysis of HCT-116 cell line after 6, 24, and 48 h of treatment with compounds **8** and **5aa**, using Annexin V/7-AAD. DMSO and Etoposide were used as reference compounds. Representative dot-plot analyses are shown in the left panels (**A**), and quantitation of analysis is presented in the right panels (**B**). (**C**) Microscopic images obtained after 48 h of treatment with the indicated compounds and staining with Annexin V. Modulation of caspase-3/7 in HCT-116 cells after treatment with compounds are presented on representative histograms (**D**) and bar charts (**E**). Error bars represent the SEM of data obtained in n=3 independent experiments. Statistical differences were analyzed with a two-way ANOVA. $^{ns}p>0.05$, $*p<0.01$, $**p<0.001$, $***p<0.0001$ vs. vehicle.

2.2.6. Effect of carbazole analogs on mitochondrial ROS generation

ROS (reactive oxygen species) play a pivotal role in activating cell death pathways.[38] To study the impact of **5aa** and **8** on oxidative stress, intracellular ROS production in HCT-116 cells treated with these compounds was analyzed using an H2DCFDA probe. The results showed that compound **5aa** caused persistent, but mostly insignificant ROS generation in HCT-116 cells, whereas exposure to **8** induced a rapid and persistent increase of ROS (**Figure 8A** and **Figure 8C**). A 15-μM concentration of **8** induced tremendous accumulation of ROS

(64.2±7.7% positive cells, 24 h; ***p<0.001) relative to 5aa (19.6±7.3% positive cells, 24 h; *p<0.05) in HCT-116 cell line. Dysregulation of redox homeostasis could lead to cell death, including apoptosis and autophagy. To study whether the elevated ROS level was the primary cause of death in cells exposed to compound **8**, they were pretreated with N-acetyl-L-cysteine (NAC), a known antioxidant and ROS scavenger. It was observed that NAC diminished ROS generation induced by compound 8 in HCT-116 cell line (**Figure S3** and **Figure S4**, Supplementary Information). This implied that NAC restored the cellular redox balance which was primarily altered by **8**. To study the general applicability of ROS generation caused by tested compounds in other cancers, changes of ROS were also investigated in the U-2 OS cell line (**Figure 8B** and **Figure 8D**). The results revealed that both compounds caused similar time-dependent accumulation of ROS, but this effect was reduced after treatment with **8** in comparison to HCT-116 cells. The level of induced ROS was found to be abolished after NAC pretreatment, as also observed in HCT-116 cells (**Figure 5** and **Figure S6**, Supplementary Information. Taken together, it seems that cellular stress is of importance in the anticancer activity of these novel carbazole analogs.
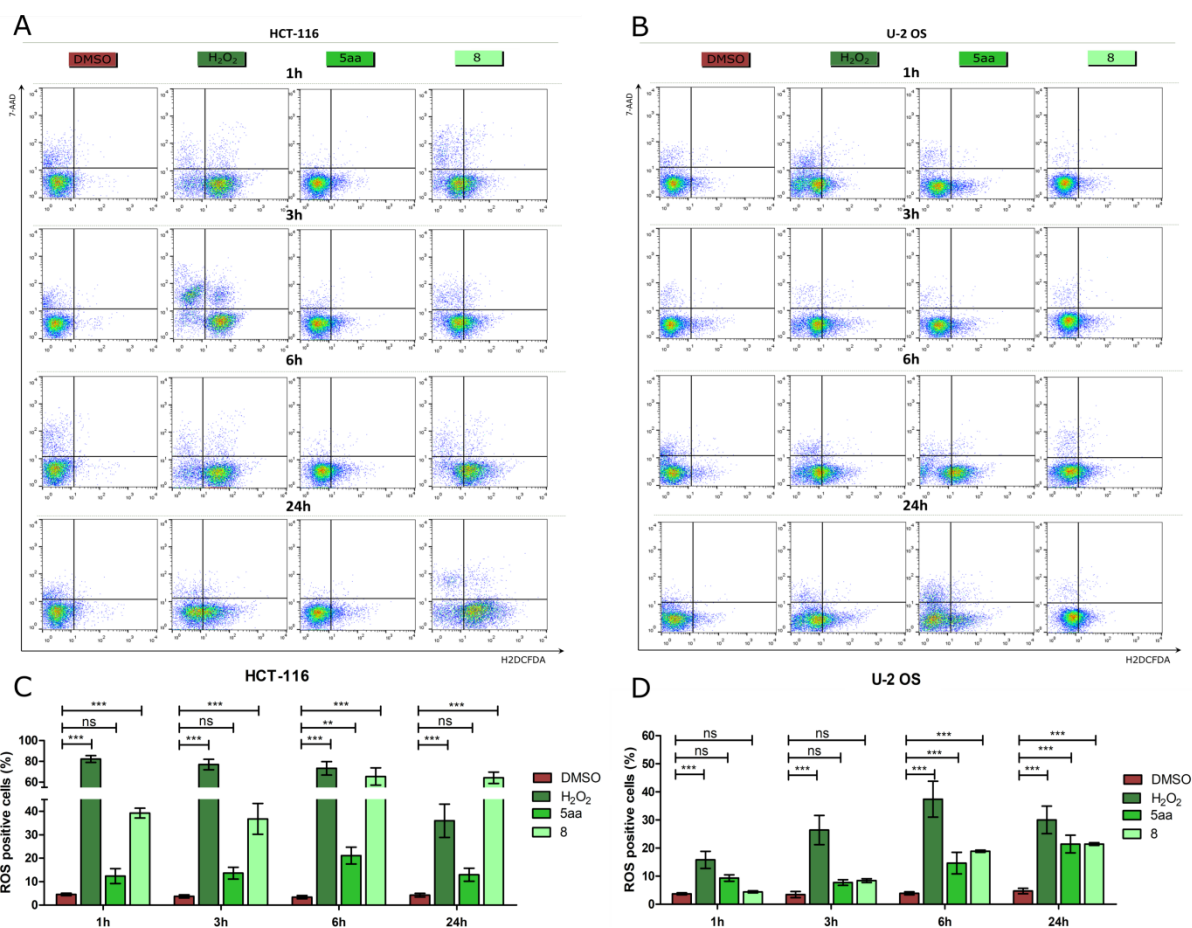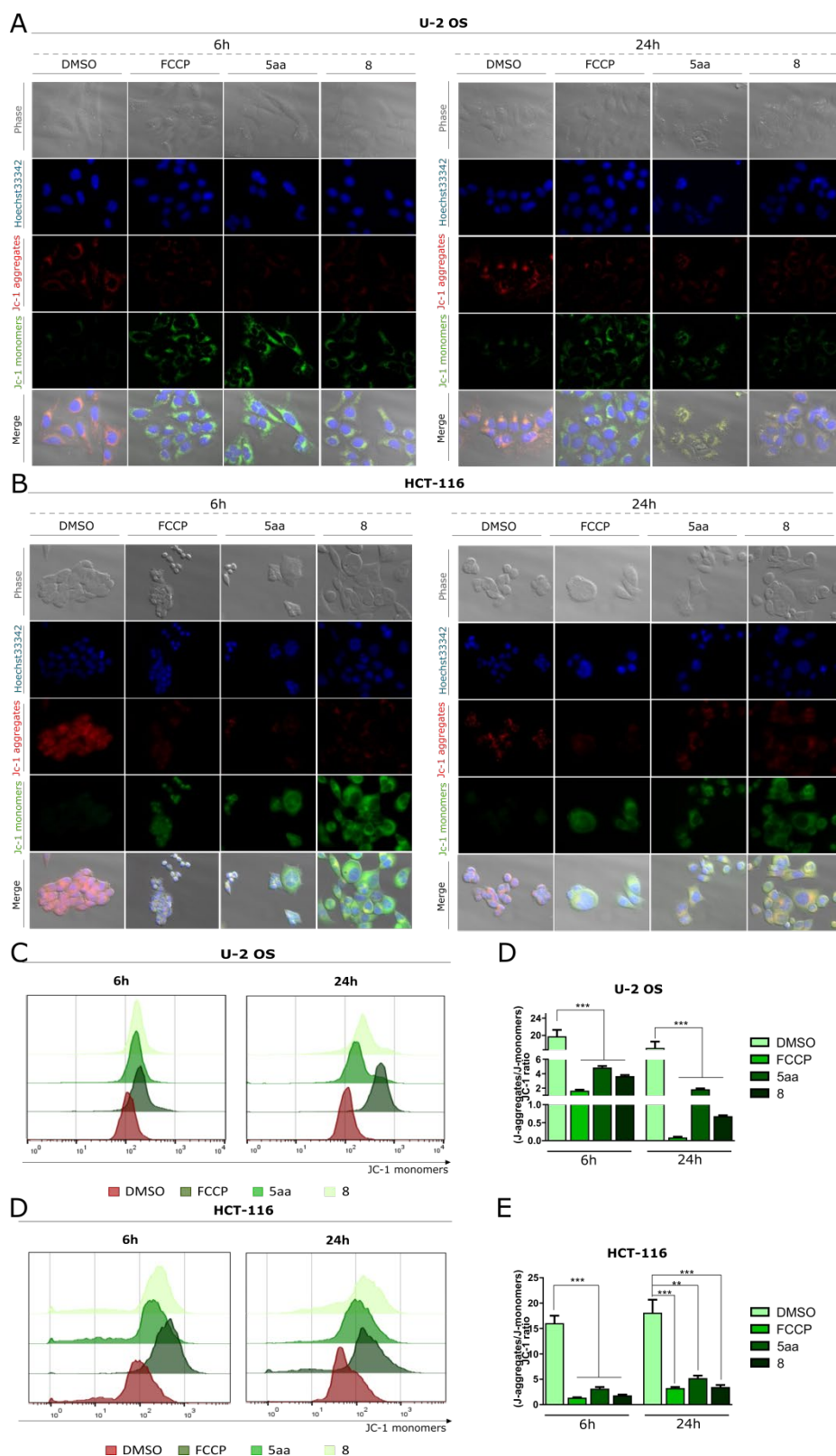
Figure 8 Flow cytometric analyses of ROS induction in HCT-116 (**A**) and U-2 OS (**B**) cells after 1, 3, 6, and 24 h of treatment with compounds **8** and **5aa**, using H$_2$DCFDA probe. DMSO and H$_2$O$_2$ were used as reference compounds. The quantitation of analysis is presented in (**C**) and (**D**). Error bars represent the SEM of data obtained in n=4 independent experiments. Statistical differences were analyzed with a two-way ANOVA. $^{ns}p>0.05$, $^{**}p<0.001$, $^{***}p<0.0001$ vs. vehicle.

*2.2.7. Changes in mitochondrial morphology in HCT-116 cell line after treatment with **5aa** and **8***

Overproduction of ROS can influence mitochondrial functions and initiate mitochondrial-mediated cell death via loss of mitochondrial transmembrane potential ($\Delta\Psi$m) in cancer cells.[39] Therefore, we monitored $\Delta\Psi$m using a 5,5,6,6′-tetrachloro-1,1′,3,3′-tetraethylbenzimi-dazoylcarbocyanine iodide (JC-1) fluorescent probe. In apoptotic or necrotic cells, mitochondria sequester the red-fluorescent JC-1 aggregate and diffuse it out in monomeric form to the cytosol, emitting green fluorescence. [40] **Figure 9** shows the representative histograms of JC-1-stained HCT-116 and U-2 OS cells, and the aggregate/monomer ratio determined by flow cytometry in different treated groups. The

results obtained from stained cells showed a significant time-dependent reduction of $\Delta\Psi$m in both **5aa**- and **8**-treated HCT-116 and U-2 OS cells. Furthermore, the observed loss of $\Delta\Psi$m induced by **8** was higher compared to **5aa** after treatment for a short time (6 h) indicating a decrease in the aggregate/monomer ratio (1.83±0.24 and 3.18±0.44, respectively) as compared to control. However, after exposure to **5aa** and **8** for 24 h, the polarization of mitochondrial membrane was restored in HCT-116 cells, but only partially. The collapse of $\Delta\Psi$m has often been viewed as a point of no return in cell death. [41] Moreover, $\Delta\Psi$m maintains a driving force for energy production, and a gradual loss of this potential can disrupt the coupling efficiency between phosphorylation and oxidation, resulting in considerable bioenergetic deficits. Besides the loss of ATP production through aerobic respiration, maintenance of $\Delta\Psi$m is required for the import of several mitochondrial proteins that affect different mitochondrial functions. [42]

Figure 9 Analysis of ΔΨm. JC-1 staining images of HCT-116 (**A**) and U-2 OS (**D**) cells acquired after 6 and 24 h of treatment with **5aa** and **8**. FCCP was used as a reference. Flow cytometric analyses of JC-1 staining are presented on representative histograms (**B**, **E**) and bar charts with statistical quantifications of JC-1 ratio (J-aggregates/J-monomers) (**C**, **F**). Data represent the mean±SEM of at least n=4 independent experiments. Statistical differences were analyzed with a Bonferroni post hoc test. **$p<0.0001$, ***$p<0.0001$ compared with control (DMSO).

Previous studies have shown that mitochondrial morphology is a sensitive indicator of the action of some chemotherapeutics and changes occur in morphology before cell death. [43,44] In addition to mitochondrial outer membrane permeabilization, the mitochondrial network succumbs to substantial fragmentation caused by decreased fusion and elevated mitochondrial fission. [45] Therefore, we investigated the influence of the studied compounds on mitochondrial phenotype. After treatment, the mitochondria of cells were visualized by confocal microscopy after labeling with mitochondria-targeted cationic dye MitoTracker Green and staining with DNA minor groove-binding ligand Hoechst 33342 (**Figure 10A**). The results indicated that mitochondrial morphology was altered in cells exposed to both tested compounds **8** and **5aa** after 6 h of treatment and the cells showed a tendency to form short (**Figure 10C**), circular-shaped (**Figure 10E**) mitochondria, all of which are consistent with increased fission. [46] Compound **8** caused a stronger reduction in mitochondrial length than **5aa** ($50.34\pm8.47\%$ and $36.71\pm7.61\%$, respectively; $**p<0.001$), in comparison to the control. Quantification of mitochondrial morphology also revealed an increased number of mitochondria (**Figure 10B**) and a reduction in the average size of mitochondria (**Figure 10D**), which suggests massive swelling of fragmented mitochondria. Both tested compounds induced the release of mitochondrial DNA into the cytosol by increasing the permeabilization of the mitochondrial inner membrane, which could potentially lead to cell death-associated inflammation.[47] The observed alterations in mitochondrial phenotype were probably reflected by oxidative stress caused by treatment with the studied compounds.
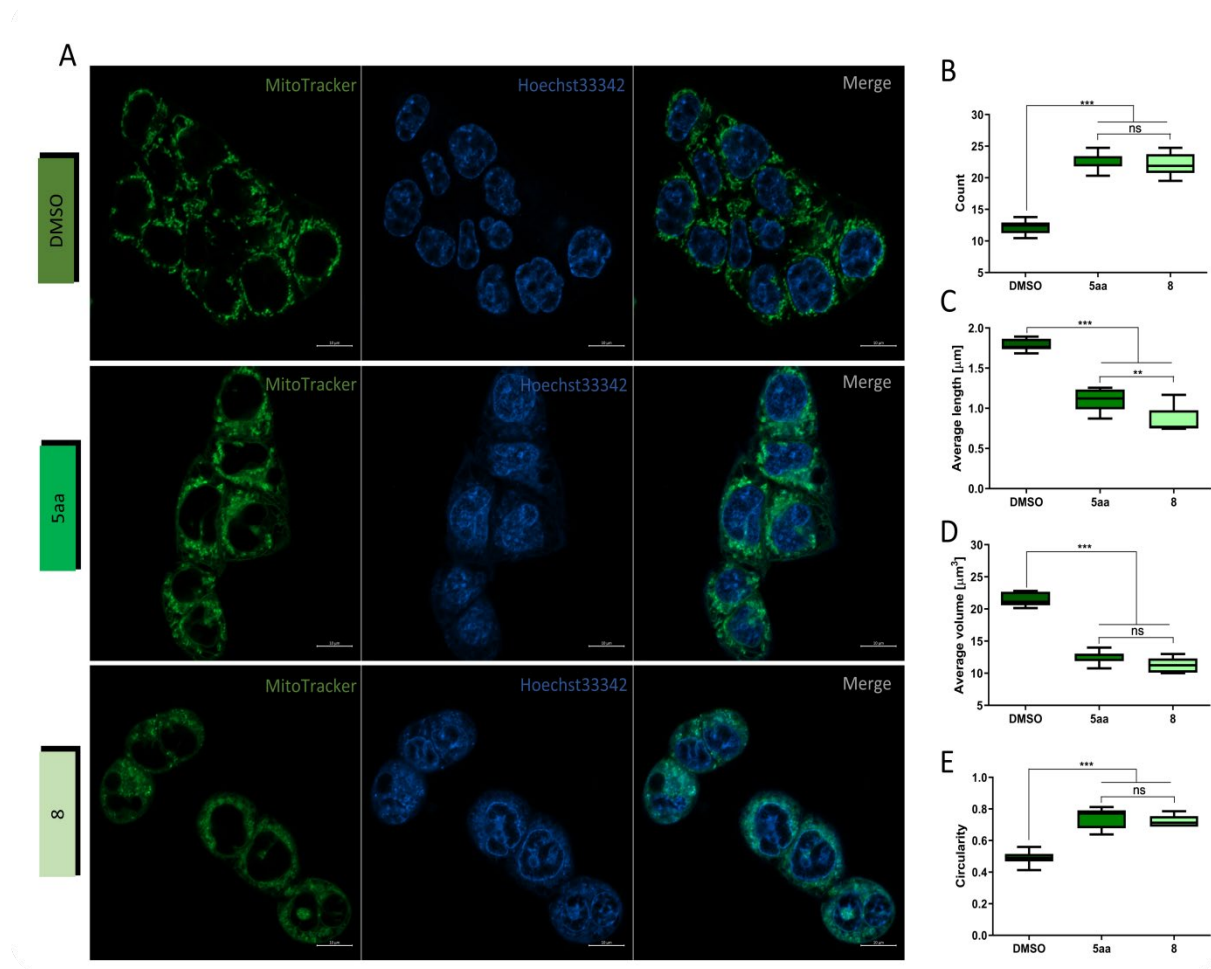
Figure 10 Quantitative mitochondrial morphometric analyses. (**A**) Representative confocal images of the mitochondrial morphology of HCT-116 cells acquired after 6 h of treatment with compounds **5aa** and **8**, and with DMSO (scale bar=10 µm); Green—MitoTracker, blue—Hoechst 33342. (**B**) Number of counted mitochondrial particles. (**C**) Average length (µm) and (**D**) volume (µm^3) of mitochondria. (**E**) Circularity of mitochondria (index of elongation). Statistical quantification of mitochondrial morphology was performed based on Z-axis confocal stacks. Data represent mean±SEM of at least n=4 independent experiments. Statistical differences were analyzed with a Bonferroni post hoc test. ***p<0.0001, **p<0.001 compared with control (DMSO).

2.2.8. Oxidative DNA damage

Elevated intracellular levels of ROS lead to the oxidization of nucleotides, thereby inducing DNA double-strand breaks (DSBs) in a replication-dependent manner. [39] Therefore, we investigated the phosphorylation of H2AX at Ser 139, a marker of DSB, in treated HCT-116 and U-2 OS cell lines. As shown in **Figure 11**, **5aa** and **8** caused a comparable increase in H2AX phosphorylation at the early stage of exposure (24 h) in HCT-116 and U-2 OS cells. In HCT-116 cell line, the level of p-H2AX remained similar after longer exposure (48 and 72 h).

However, a significant increase in the level of p-H2AX was observed at 48 h (51.0±2.8% positive cells; ***$p<0.001$) and 72 h (68.2±3.4% positive cells; ***$p<0.001$) in compound **8**-treated U-2 OS cells, but not in the cells treated with **5aa**. Massive accumulation of DNA DSBs in cells treated with **8** could be one of the mechanisms of the observed G2/M arrest in these cells.
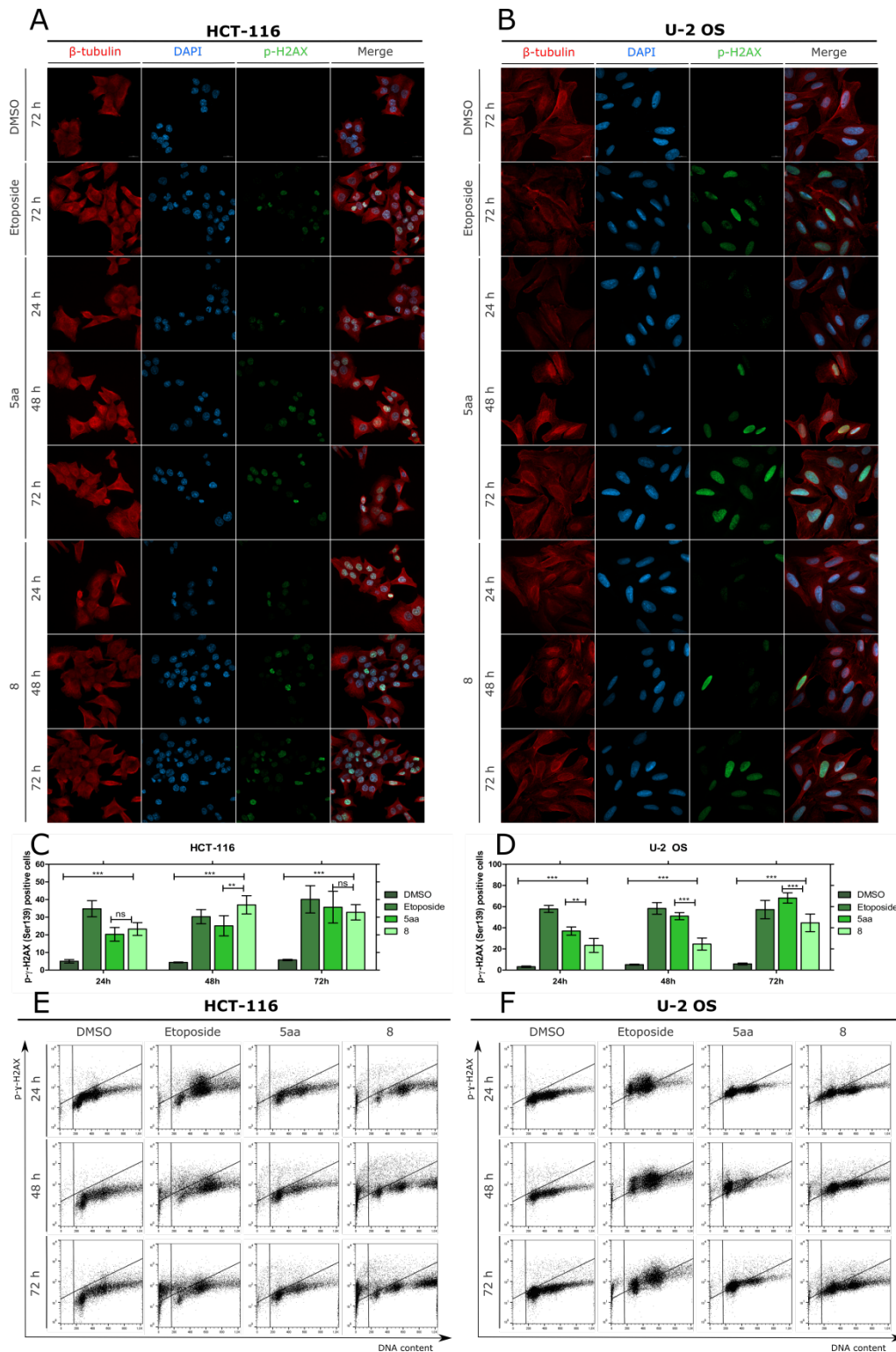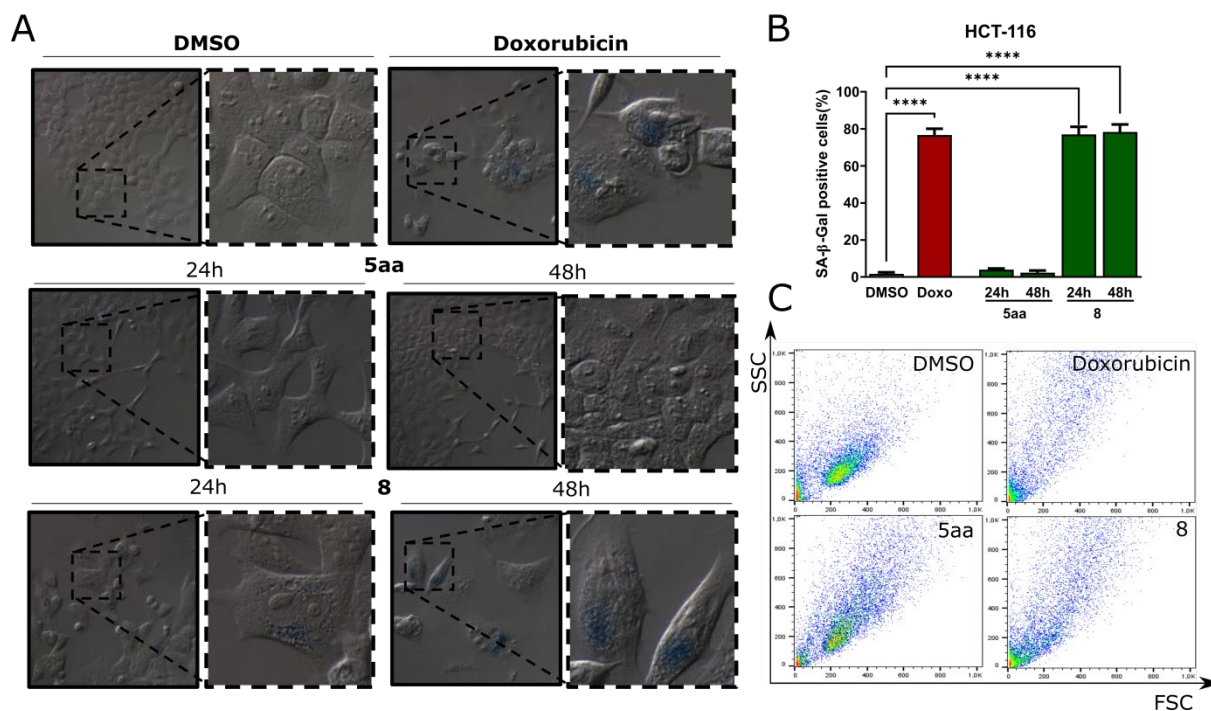
Figure 11 Representative microscopy images presenting immunofluorescence in U-2 OS (**A**) and HCT-116 (**B**) cells indicating the formation of γ-H2AX foci and changes in microtubule structure upon treatment with **5aa** and **8** (24, 48, and 72 h). Etoposide and DMSO were used as reference compounds. The microtubule is depicted in red, γ-H2AX in green, and nucleus in blue (DAPI). Scale bars=100 μm. (**C**, **D**) Representative dot-plot diagrams after flow cytometric analyses of p-γ-H2AX staining. (**E**) Quantification showing the average percent of p-γ-H2AX-positive cells plotted as a bar graph depicting mean±SEM. Error bars represent the SEM of data obtained in n=3 independent experiments. Statistical differences were analyzed with a two-way ANOVA.

2.2.9. Induction of cell senescence

Treatment with different doses of drugs may promote the suppression of carcinoma through different mechanisms. However, a low concentration of drugs may result in the induction of premature senescence rather than cell death.[48] Therefore, we examined the accumulation of the molecular markers of stress-induced premature senescence in cells treated with **5aa** and **8** for 24 and 48 h. For this purpose, the cells were washed, cultured for an additional 96 or 72 h, and stained with x-gal. It was observed that compound **8** induced cellular senescence in HCT-116 cells in all treatment time points, similar to the positive control (Doxorubicin), which indicates the high activity of senescence-associated β-galactosidase (SA-β-Gal) (**Figure 12A** and **Figure 12B**), as well as flattening and enlargement of cells (Figure 12C). On the other hand, the morphology of **5aa**-treated cells did not change during cultivation in comparison to vehicle. Similar results were obtained in the case of U-2 OS cells, except that the activity of SA-β-Gal did not increase after treatment (**Figure S7**, Supplementary Information).

Figure 12 (**A**) (**A**) Representative microscopy images showing SA-β-Gal staining and morphology of HCT-116 cells acquired after 24 or 48 h of treatment with the investigated compounds (10 μM **5aa**, 10 μM **8**) and prolonged culturing for 96 or 72 h. Doxorubicin was used as a reference compound. (**B**) Quantification showing the average percent of SA-β-Gal-positive cells plotted as a bar graph depicting mean±SEM. (**C**) Representative dot-plot analyses after 48 h of treatment with the investigated compounds (10 μM **5aa**, 10 μM **8**) and prolonged culturing for 96 h. Error bars represent the SEM of data obtained in n=10 random fields of view. Statistical differences were analyzed with a two-way ANOVA. ***$p<0.0001$ vs. vehicle.

3. Conclusion

In summary, a novel series of anticancer compounds based on a substituted carbazole scaffold were synthesized. The application of a recently developed method of synthesis allowed convenient formation of three or four substituted aminocarbazoles from oxopentanoate tryptophan derivatives in a three-step process. Among the synthesized carbazole derivatives, compounds **5aa** and **8** were found to be the most active, which effectively inhibited the growth of HCT-116 and U-2 OS cells compared with 5-fluorouracil used as reference compound. Compound **8** showed a 3–6 times higher anticancer activity against these cell lines than compound **5aa**, which indicates that the structural modification of compound **5aa** led to the discovery of a compound with better anticancer properties. Annexin-V staining revealed

that treatment with both compounds for 6–48 h induced 10–40% ($p<0.05$) apoptotic cell death in HCT-116 cell line, while negligible change occurred in apoptosis in U-2 OS cell line. Compound **8** induced intense senescence in both HCT-116 and U-2 OS cell lines. This reveals that both compounds exhibited a different mechanism of action depending on the cell line. Furthermore, they displayed a potent oxidative effect in HCT-116 and U-2 OS cells, inducing massive accumulation of DNA DSBs, which led to a parallel change in the assembly of mitochondria causing their dysfunction. These findings are expected to provide new leads for the treatment of colon cancer and osteosarcoma.

4. Experimental section

General: Commercially available reagents were purchased from Sigma-Aldrich or Acros and used without further purification. THF was distilled in the presence of potassium under argon shortly before use. DCM was distilled over P_4O_{10} and stored over molecular sieves. The reagents 2-((tert-butoxycarbonyl)amino)-3-(1H-indol-3-yl)propanoic acid (**3aa**),[29] 2-((ethoxycarbonyl)amino)-3-(1H-indol-3-yl)propanoic acid (**3ab**),[27] 2-acetamido-3-(1H-indol-3-yl)propanoic acid (**3ac**),[26] 2-(((benzyloxy)carbonyl)amino)-3-(1H-indol-3-yl)propanoic acid (**3ad**),[28] and 2-(1,3-dioxoisoindolin-2-yl)-3-(1*H*-indol-3-yl)propanoic acid (**3ae**)[25] were prepared as described in the literature. Analytical thin-layer chromatography was performed on aluminum sheets of UV-254 Merck silica gel, and flash chromatography using SilicaFlash P60 silica gel (40–63 μm). ^{1}H and ^{13}C NMR spectra were recorded with Bruker Avance III HD 400 MHz, and NMR chemical shifts were reported in δ (ppm) using residual solvent peaks as standards with the coupling constant J measured in Hz. High-resolution mass spectra were recorded with an Agilent 6540 Q-TOF system. Melting points were determined with a Warsztat Elektromechaniczny W-wa apparatus and were used uncorrected.

Boc-protected tryptophans. General procedure.[29]

To a solution of **2b-c** (10 mmol) and NaHCO$_3$ (1.64 g, 19 mmol) in a dioxane:water 1:1 mixture (20 ml) at 0°C di-tert-butyl dicarbonate (3.37 ml, 15 mmol) was added in one portion. The reaction mixture was stirred 13 h at R.T concentrated in a vacuum. The residue was washed with AcOEt (2 x 15 ml) and discarded. The water layer was acidified to pH = 3 with 5% aqueous HCl and extracted with AcOEt (2 x 15 ml), organic extract was dried with MgSO$_4$ filtered and evaporated to dryness under reduced pressure. The crude products were used without additional purification.

In the case of 5-hydroksytryptophane **2c**, the crude product was subject to additional O-acetylation with the following procedure.

Crude N-Boc-5-hydroksytryptophane (100 mg, 0.31 mmol) was dissolved in 1N NaOH (0.7 ml) and acetic anhydride was added (63 μl, 0.67 mmol). The reaction mixture was stirred for 3 h at R. T. under argon. The solution was acidified with 5 % citric acid and extracted with AcOEt (3 x 5 ml), organic extract was washed with brine (5 ml), dried with MgSO$_4$ filtered, and evaporated to dryness under reduced pressure. The crude products were used without additional purification.

2-((tert-butoxycarbonyl)amino)-3-(5-((tert-butoxycarbonyl)amino)-1H-indol-3-yl)propanoic acid (3ba)

Colorless oil; yield 98%; ^{1}H NMR (400 MHz, CDCl$_3$, δ): 8.54 (bs, 1H), 7.54 (bs, 1H), 7.13-7.05 (m, 2H), 6.88 (s, 1H), 6.76-6.69 (m, 1H), 5.23-5.11 (m, 1H), 4.62-4.60 (m, 1H), 3.20-3.04 (m, 2H), 1.55 (s, 9H), 1.43 (s, 9H); ^{13}C NMR (100 MHz, CDCl$_3$, δ): 175.6, 171.3, 155.6, 133.3, 130.1, 127.8, 124.2, 116.5, 111.4, 110.6, 109.6, 80.0, 53.9, 28.5, 28.4; HRMS (ESI+): m/z [M + H]$^+$ calcd for C$_{21}$H$_{30}$N$_3$O$_6$, 420.2135; found, 420.2157.

3-(5-acetoxy-1H-indol-3-yl)-2-((tert-butoxycarbonyl)amino)propanoic acid (3ca)

Colorless oil; yield 39%; ^{1}H NMR (400 MHz, CDCl$_3$, δ): 8.46 (s, 1H), 7.29-7.25 (m, 2H), 6.92-6.87 (m, 2H) 5.17-5.15 (m, 1H), 4.64-4.63 (m, 1H), 3.31-3.18 (m, 2H), 2.33 (s, 3H), 1.46 (s, 9H); ^{13}C NMR (100 MHz, CDCl$_3$, δ): 172.1, 171.4, 166.2, 150.8, 139.4, 129.3, 123.4,

119.9, 111.4, 107.0, 106.1, 75.5, 55.7, 23.6, 23.3, 16.4; HRMS (ESI+): m/z [M + Na]$^+$ calcd for $C_{18}H_{22}N_2O_6Na$, 385.1375; found, 385.1397.

General procedure for preparation of ethyl 5-(1H-indol-3-yl)-3-oxopentanoate derivatives (4aa-ca)

To a solution of N-protected Trp **3aa-ca** (0.59 mmol) in dry THF (12 ml) carbonyldiimidazole (106 mg, 0.65 mmol) was added. The resulting mixture was stirred for 2 h at R.T under argon. Then MgCl$_2$ (56 mg, 0.59 mmol) was added following by ethyl potassium malonate (100 mg, 0.59 mmol). The resulting reaction mixture was stirred for 1 h at R.T under argon and then was heated to 40-45°C stirred for an additional 12 h. After completion of the reaction, the mixture was filtered and concentrated in vacuum. The residue was purified with flash chromatography as specified below.

Ethyl 4-((tert-butoxycarbonyl)amino)-5-(1H-indol-3-yl)-3-oxopentanoate (4aa)

Purification by flash column chromatography (EtOAc/Hex, 1:3). White amorphous solid; yield 44%; ^{1}H NMR (400 MHz, CDCl$_3$, δ): 8.23 (s, 1H), 7.65-7.63 (m, 1H), 7.40-7.37 (m, 1H), 7.25-7.22 (m, 1H), 7.20-7.12 (m, 1H), 7.04-7.03 (m, 1H), 5.18-5.16 (m, 1H), 4.74-4.69 (m, 1H), 4.18-4.13 (m, 2H), 3.51 (d, *J* = 16.0 Hz, 1H), 3.44 (d, *J* = 16.0 Hz, 1H), 3.34-3.22 (m, 2H), 1.44 (s, 9H), 1.26 (t, *J* = 8.0 Hz, 3H); ^{13}C NMR (100 MHz, CDCl$_3$, δ): δ= 202.7, 167.0, 155.4, 136.2, 127.5, 123.0, 122.3, 119.8, 118.8, 111.2, 110.0, 80.1, 61.4, 59.9, 47.0, 28.3, 26.9, 14.0; HRMS (ESI+): m/z [M + Na]$^+$ calcd for $C_{18}H_{22}N_2O_6Na$, 397.1738; found, 397.1692.

Ethyl 4-((ethoxycarbonyl)amino)-5-(1H-indol-3-yl)-3-oxopentanoate (4ab)

Purification by flash column chromatography (EtOAc/Hex, 1:2). Colorless oil; yield 16%; ^{1}H NMR (400 MHz, CDCl$_3$, δ): 8.27 (s, 1H), 7.66-7.64 (m, 1H), 7.39-7.36 (m, 1H), 7.25-7.20 (m, 1H), 7.20-7.13 (m, 1H), 7.03 (s, 1H), 5.36 (d, *J* = 7.2 Hz, 1H), 4.81-4.76 (m, 1H),4.18-4.10 (m, 4H), 3.50 (d, *J* = 16.0 Hz, 1H), 3.44 (d, *J* = 16.0 Hz, 1H), 3.34-3.25 (m, 2H), 1.27-

1.22 (m, 6H); ^{13}C NMR (100 MHz, CDCl$_3$, δ): 202.4, 166.9, 156.2, 136.2, 127.4, 123.1, 122.4, 119.9, 118.7, 111.3, 109.8, 61.5, 60.1, 47.2, 27.1, 14.0; HRMS (ESI+): m/z [M + H]$^+$ calcd for C$_{18}$H$_{23}$N$_2$O$_5$, 347.1607; found, 347.1614.

Ethyl 4-acetamido-5-(1H-indol-3-yl)-3-oxopentanoate (4ac)

Purification by flash column chromatography (EtOAc/Hex, 1:3). Yellow amorphous solid; yield 46%; ^{1}H NMR (400 MHz, CDCl$_3$, δ): 8.53 (s, 1H), 7.62-7.60 (m, 1H), 7.38-7.36 (m, 1H), 7.23-7.19 (m, 1H), 7.16-7.13 (m, 1H), 7.01 (s, 1H), 6.38 (d, *J* = 7.2 Hz, 1H), 5.06-5.00 (m, 1H), 4.15 (q, *J* = 7.2 Hz, 2H), 3.50 (d, *J* = 16.0 Hz, 1H), 3.45 (d, *J* = 16.0 Hz, 1H), 3.34-3.22 (m, 2H), 1.94 (s, 3H), 1.24 (t, *J* = 7.2 Hz, 3H); ^{13}C NMR (100 MHz, CDCl$_3$, δ): 201.9, 170.5, 166.9, 136.2, 127.5, 123.1, 122.3, 119.8, 118.5, 111.5, 109.5, 61.6, 58.9, 47.2, 26.6, 22.9, 14.0; HRMS (ESI+): m/z [M + H]$^+$ calcd for C$_{17}$H$_{21}$N$_2$O$_4$, 317.1501; found, 317.1495.

Ethyl 4-(((benzyloxy)carbonyl)amino)-5-(1H-indol-3-yl)-3-oxopentanoate (4ad)

Purification by flash column chromatography (EtOAc/Hex, 1:3). Yellow amorphous solid; yield 28%; ^{1}H NMR (400 MHz, CDCl$_3$,): δ = 8.19 (s,1 H), 7.63 (d, *J* = 7.6 Hz, 1 H), 7.42-7.30 (m, 6 H), 7.26-7.20 (m, 1 H), 7.17-7.12 (m, 1 H), 7.01-6.95 (m, 1 H), 5.48 (d, *J* = 7.6 Hz, 1 H), 5.12 (s, 2 H), 4.82 (dd, *J* = 13.6 Hz, *J* = 6.4 Hz, 1 H), 4.15 (q, *J* = 7.2 Hz, 2 H), 3.50 (d, *J* = 16.0 Hz, 1 H), 3.44 (d, *J* = 16.0 Hz, 1 H), 3.56-3.40 (m, 2 H), 3.35-3.25 (m, 2H), 1.24 (t, *J* = 6.8 Hz, 3 H).

Ethyl 4-(1,3-dioxoisoindolin-2-yl)-5-(1H-indol-3-yl)-3-oxopentanoate (4ae)

Purification by flash column chromatography (EtOAc/Hex, 1:3). Yellow amorphous solid; yield 25%; ^{1}H NMR (400 MHz, CDCl$_3$,): δ = 7.98 (bs, 1 H), 7.79-7.75 (m, 2 H), 7.69-7.65 (m, 2 H), 7.64-7.62 (m, 1 H), 7.29-7.27 (m, 1 H), 7.17-7.12 (m, 1 H), 7.10-7.05 (m, 1 H), 7.03 (d, *J* = 2 Hz, 1 H), 5.30 (dd, *J* = 10.0 Hz, *J* = 6.0 Hz, 1 H), 4.22-4.16 (m, 2 H), 3.84-3.73 (m, 2 H), 1.72-1.64 (m, 2 H), 0.92 (t, *J* = 7.6 Hz, 3 H).

Ethyl 4-((tert-butoxycarbonyl)amino)-5-(5-((tert-butoxycarbonyl)amino)-1H-indol-3-yl)-3-oxopentanoate (4ba)

Purification by flash column chromatography (EtOAc/Hex, 1:2). Colorless oil; yield 43%; ^{1}H NMR (400 MHz, CDCl$_3$,): δ = 8.36 (s, 1 H), 7.53 (s, 1 H), 7.27-7.23 (m, 1 H), 7.23-7.19 (m, 1 H), 6.97 (s, 1 H), 6.59 (s, 1 H), 5.17 (d, J = 7.6 Hz, 1 H), 4.67-4.62 (m, 1 H),4.18-4.13 (m, 2 H), 3.50 (d, J = 16.0 Hz, 1 H), 3.43 (d, J = 16.0 Hz, 1 H), 3.25-3.14 (m, 2 H), 1.55 (s, 9 H), 1.42 (s, 9 H), 1.30-1.23 (m, 3 H). ^{13}C NMR (100 MHz, CDCl$_3$): δ= 202.8, 167.0, 155.4, 153.7, 133.2, 130.9, 127.6, 124.0, 116.4, 111.5, 109.8, 109.5, 80.1, 61.4, 59.8, 47.0, 28.4, 26.9, 14.1. HRMS (ESI+): m/z [M + H]$^+$ calcd for C$_{25}$H$_{36}$N$_3$O$_7$: 490.2552; found: 490.2574

Ethyl 5-(5-acetoxy-1H-indol-3-yl)-4-((tert-butoxycarbonyl)amino)-3-oxopentanoate (4ca)

Purification by flash column chromatography (EtOAc/Hex, 1:2). Colorless oil; yield 49%; ^{1}H NMR (400 MHz, CDCl$_3$, δ): 8.38 (s, 1H), 7.53-7.31 (m, 2H), 7.01 (s, 1H), 6.94-6.91 (m, 1H), 5.16 (d, J = 7.2 Hz, 1H), 4.68-4.63 (m, 1H), 4.19-4.12 (m, 2H), 3.52 (d, J = 16.0 Hz, 1H), 3.45 (d, J = 16.0 Hz, 1H), 3.28-3.15 (m, 2H), 2.34 (s, 3H), 1.44 (s, 9H), 1.30-1.24 (m, 3H); ^{13}C NMR (100 MHz, CDCl$_3$, δ): 202.4, 170.5, 167.0, 155.3, 144.4, 134.0, 127.9, 124.5, 116.5, 111.8, 110.8, 110.3, 80.0, 61.5, 59.9, 46.9, 28.3, 26.7, 21.2, 14.1; HRMS (ESI+): m/z [M + H]$^+$ calcd for C$_{22}$H$_{29}$N$_2$O$_7$, 433.1975; found, 433.1981.

*General procedure for oxidative cyclization of 3-oxoesters **4aa-ca** with Mn(OAc)$_3$*2 H$_2$O*

Ester **4aa-ca** (0.1 mmol) was dissolved in AcOH (2 ml). To a resulted solution Mn(OAc)$_3$*2 H$_2$O (67 mg, 0.25 mmol) was added. The resulting mixture was heated for 2.5 h at 70°C. After completion of the reaction, the solvent was removed under vacuum, and the residue was purified with flash chromatography as specified below.

*General procedure for oxidative cyclization of 3-oxoesters **4aa-ae** with transition metal triflates*

Ester **4aa-ae** (0.2 mmol) was dissolved in anhydrous DCM (4 ml). A resulting solution (0.4 mmol) of metal triflate specified in Table 1 was added, followed by I$_2$ (0.3 mmol) and NEt$_3$ (0.5 mmol, 69 μL). The resulting mixture was stirred for 12 h at R.T. After completion of the reaction, the residue was dissolved in DCM (30 mL) and washed with aqueous sat. Na$_2$SO$_3$.

The organic layer was dried with MgSO$_4$, the solvent was removed under vacuum, and the residue was purified with flash chromatography as specified below.

*Ethyl 3-((tert-butoxycarbonyl)amino)-2-hydroxy-9H-carbazole-1-carboxylate (**5aa**)*

Purification by flash column chromatography (EtOAc/Hex, 1:5). Yellow amorphous solid; yield 67%; ^{1}H NMR (400 MHz, CDCl$_3$, δ): 11.60 (s, 1H), 9.01 (s, 1H), 8.97 (s, 1H), 8.02 (d, *J* = 7.6 Hz, 1H), 7.46-7.44 (m, 1H), 7.40-7.36 (m, 1H), 7.27-7.23 (m, 1H), 7.14 (s, 1H), 4.66 (q, *J* = 7.2 Hz, 2H), 1.61 (t, *J* = 7.2 Hz, 3H), 1.60 (s, 9H); ^{13}C NMR (100 MHz, CDCl$_3$, δ): 170.5, 153.3, 150.8, 138.6, 133.9, 124.7, 123.3, 120.7, 120.0, 119.7, 116.9, 115.4, 110.6, 96.2, 80.3, 62.2, 28.5, 14.6; HRMS (ESI+): m/z [M]$^+$ calcd for C$_{20}$H$_{22}$N$_2$O$_5$, 370.1528; found, 370.1481.

*Ethyl 3-((ethoxycarbonyl)amino)-2-hydroxy-9H-carbazole-1-carboxylate (**5ab**)*

Purification by flash column chromatography (EtOAc/Hex, 1:5). Yellow amorphous solid; yield 28%; ^{1}H NMR (400 MHz, CDCl$_3$, δ): δ = 11.56 (s, 1H), 8.96 (s, 1H), 8.92 (s, 1H), 7.98 (d, *J* = 8.0 Hz, 1H), 7.44-7.42 (m, 1H), 7.40-7.36 (m, 1H), 7.26-7.20 (m, 2H), 4.63 (q, *J* = 7.2 Hz, 2H), 4.32 (q, *J* = 7.2 Hz, 2H), 1.59 (t, *J* = 7.2 Hz, 3H), 1.40 (t, *J* = 7.2 Hz, 3H); ^{13}C NMR (100 MHz, CDCl$_3$, δ): 170.4, 154.1, 150.9, 138.7, 134.1, 124.8, 123.2, 120.2, 120.1, 119.6, 117.0, 115.4, 110.6, 96.2, 62.2, 61.2, 14.7, 14.6; HRMS (ESI+): m/z [M + H]$^+$ calcd for C$_{18}$H$_{19}$N$_2$O$_5$, 343.1294; found, 343.1277.

*Ethyl 3-acetamido-2-hydroxy-9H-carbazole-1-carboxylate (**5ac**)*

Purification by flash column chromatography (EtOAc/Hex, 1:2). Yellow amorphous solid; yield 29%; ^{1}H NMR (400 MHz, CDCl$_3$, δ): 11.65 (s, 1H), 9.19 (s, 1H), 9.01 (s, 1H), 8.00 (d, *J* = 7.6 Hz, 1H), 7.80 (s, 1H), 7.45-7.43 (m, 1H), 7.40-7.36 (m, 1H), 7.27-7.24 (m, 1H), 4.64 (q, *J* = 7.2 Hz, 2H), 2.29 (s, 3H), 1.60 (t, *J* = 7.2 Hz, 3H); ^{13}C NMR (100 MHz, CDCl$_3$, δ): 170.5, 168.3, 151.0, 138.7, 134.5, 124.9, 123.2, 120.2, 119.8, 118.6, 115.4, 110.6, 96.1, 62.3, 24.8, 14.6; HRMS (ESI+): m/z [M + H]$^+$ calcd for C$_{17}$H$_{17}$N$_2$O$_4$, 313.1187; found, 313.1165.

*Ethyl 3,6-bis((tert-butoxycarbonyl)amino)-2-hydroxy-9H-carbazole-1-carboxylate (**5ba**)*

Purification by flash column chromatography (EtOAc/Hex, 1:4). Colorless oil; yield 36 %; [^1]H NMR (400 MHz, CDCl$_3$, δ): 11.61 (s, 1H), 8.91 (s, 1H), 8.87 (s, 1H), 7.97 (s, 1H), 7.35 (s, 2H), 7.09 (s, 1H), 6.56 (s, 1H), 4.65 (q, J = 7.2 Hz, 2H), 1.60 (t, J = 7.2 Hz, 3H), 1.60 (s, 9H), 1.58 (s, 9H); [^13]C NMR (100 MHz, CDCl$_3$, δ): 170.5, 166.7, 153.2, 151.1, 135.3, 134.5, 131.2, 123.6, 120.5, 117.3, 115.3, 110.6, 96.1, 80.3, 80.2, 62.2, 28.5, 14.6; HRMS (ESI+): m/z M$^+$ calcd for C$_{25}$H$_{31}$N$_3$O$_7$, 485.2162; found, 485.2173.

Ethyl 6-acetoxy-3-((tert-butoxycarbonyl)amino)-2-hydroxy-9H-carbazole-1-carboxylate (5ca)

Purification by flash column chromatography (EtOAc/Hex, 1:4). White amorphous solid; yield 25 %; [^1]H NMR (400 MHz, CDCl$_3$, δ): 11.63 (s, 1H), 9.00 (s, 1H), 8.91 (s, 1H), 7.72-7.71 (m, 1H), 7.41-7.39 (m, 1H), 7.13-7.07 (m, 2H), 4.67 (q, J = 7.2 Hz, 2H), 2.37 (s, 3H), 1.61 (t, J = 7.2 Hz, 3H), 1.59 (s, 9H); [^13]C NMR (100 MHz, CDCl$_3$, δ): 170.4, 170.3, 153.2, 151.2, 144.4, 136.4, 134.6, 123.8, 120.9, 118.4, 116.9, 115.2, 112.4, 110.9, 96.3, 80.4, 62.3, 28.4, 21.2, 14.6; HRMS (ESI+): m/z [M + Na]$^+$ calcd for C$_{22}$H$_{24}$N$_2$O$_7$Na, 451.1480; found, 451.1455.

General procedure for preparation of ethyl 3-(5-alkylfuran-2-carboxamido)-2-hydroxy-9H-carbazole-1-carboxylate derivatives (7aa-ba)

Compound **5aa** or **5ba** (0.135 mmol) was dissolved in dry DCM (1ml) and TFA 0.5 ml was added. The reaction mixture was stirred and monitored with TLC until the substrate disappears. Then solvents were removed under reduced pressure, and the residue was evaporated three times with 3 ml of toluene. Crude trifluoroacetic acid salts of **6aa** or **6ba** were used for the next step without purification.

Residue was dissolved in DMF (2 ml), and 5-metylfuran-2-carboxylic acid or 5-ethylfuran-carboxylic acid (0.135 mmol) was added followed by NEt$_3$ (225 µL, 1.63 mmol) and TBTU (53 mg, 0.163 mmol). The reaction mixture was stirred for 18h at R. T. Solvent was removed under reduced pressure, the residue was purified with flash chromatography as specified below.

*Ethyl 2-hydroxy-3-(5-methylfuran-2-carboxamido)-9H-carbazole-1-carboxylate (**7aa**)*

Purification by flash column chromatography (EtOAc/Hex, 1:3). Yellow oil; yield 15%; ^{1}H NMR (400 MHz, CDCl$_3$, δ): 10.04 (s, 1H), 9.28 (s,1H), 8.38 (s, 1H), 8.12 (d, J = 7.6 Hz, 1H), 7.52-7.46 (m, 3H), 7.31-7.27 (m, 1H), 7.15-7.14 (d, J = 3.6 Hz, 1H), 6.16-6.15 (m, 1H), 4.37 (q, J = 7.2 Hz, 2H), 2.51 (s, 3H), 1.17 (t, J = 7.2 Hz, 3H); ^{13}C NMR (100 MHz, CDCl$_3$, δ): 165.8, 158.9, 156.3, 154.7, 146.2, 142.1, 140.3, 127.0, 123.4, 122.4, 121.7, 120.8, 120.2, 118.8, 116.4, 111.1, 109.4, 105.9, 61.5, 14.2, 13.7; HRMS (ESI+): m/z [M + H]$^+$ calcd for C$_{21}$H$_{19}$N$_2$O$_5$, 379.1294; found, 379.1277.

*Ethyl 3-(5-ethylfuran-2-carboxamido)-2-hydroxy-9H-carbazole-1-carboxylate (**7ab**)*

Purification by flash column chromatography (EtOAc/Hex, 1:3). Yellow oil; yield 31%; ^{1}H NMR (400 MHz, CDCl$_3$, δ): 10.05 (s, 1H), 9.34 (s, 1H), 8.40 (s, 1H), 8.13 (d, J = 7.6 Hz, 1H), 7.53-7.52 (m, 1H), 7.50-7.46 (m, 1H), 7.32-7.28 (m, 2H), 7.17-7.16 (m, 1H), 6.16-6.15 (m, 1H), 4.37 (q, J = 7.2 Hz, 2H), 2.85 (q, J = 7.2 Hz, 2H), 1.14 (t, J = 7.2 Hz, 6H); ^{13}C NMR (100 MHz, CDCl$_3$): δ= 165.8, 164.5, 160.1, 156.4, 146.1, 141.9, 140.3, 126.7, 123.5, 122.5, 121.6, 120.8, 120.2, 118.5, 116.2, 111.1, 107.6, 105.8, 61.5, 21.5, 13.7, 11.7. HRMS (ESI+): m/z [M + H]$^+$ calcd for C$_{22}$H$_{21}$N$_2$O$_5$, 393.1449; found, 393.1426.

*Ethyl 2-((5-methylfuran-2-carbonyl)oxy)-3,6-bis(5-methylfuran-2-carboxamido)-9H-carbazole-1-carboxylate (**7ba**)*

Purification by flash column chromatography (EtOAc/Hex, 1:3). Colorless oil; yield 54%; ^{1}H NMR (400 MHz, CDCl$_3$, δ): 9.96 (s, 1H), 9.09 (s,1H), 8.33 (s, 1H), 8.23 (s, 1H), 8.21 (d, J = 1.7 Hz, 1H), 7.81 (dd, J = 8.7 Hz, J = 2.0 Hz, 1H), 7.50 (d, J = 3.4 Hz, 1H), 7.44 (d, J = 8.7 Hz, 1H), 7.18 (d, J = 3.3 Hz, 1H), 7.13 (d, J = 3.3 Hz, 1H), 6.30 (dd, J = 3.4 Hz, J = 0.8 Hz, 1H), 6.18 (dd, J = 3.3 Hz, J = 0.9 Hz, 1H), 6.14 (dd, J = 3.3 Hz, J = 0.8 Hz, 1H), 4.33 (q, J = 7.2 Hz, 2H), 2.50 (s, 3H), 2.43 (s, 3H), 2.26 (s, 3H) 1.16 (t, J = 7.2 Hz, 3H); ^{13}C NMR (100 MHz, CDCl$_3$, δ): 165.6, 158.9, 156.4, 156.3, 156.2, 157.8, 154.7, 146,5, 146.2, 142.1, 139.2, 138.2, 137.4, 130.6, 123.2, 122.3, 122.1, 121.7, 120.5, 119.3, 116.3, 116.2, 112.5, 111.5,

109.0, 108.9, 108.8, 106.0, 61.4, 14.2, 13.9, 13.8, 13.7; HRMS (ESI+): m/z [M + H]$^+$ calcd for $C_{33}H_{28}N_3O_9$, 610.1825; found, 610.1838.

*3-((tert-butoxycarbonyl)amino)-2-hydroxy-9H-carbazole-1-carboxylic acid (**8**)*

Compound **5aa** (20 mg, 0.054 mmol) was dissolved in 0.5 M solution of NaOH (H_2O:MeOH 1:1) (2 ml) and stirred for 12 h at R. T. Solution was acidified with 2 M HCl to pH = 3, and extracted with DCM (3 x 5 ml). Organic layers was washed with water (5 ml) brine (5 ml) and dried with $MgSO_4$. Solvent was removed under reduced pressure and the residue was purified with flash chromatography. (EtOAc/Hex, 1:3). White amorphous solid; yield 99%;

^{1}H NMR (400 MHz, $CDCl_3$, δ): 11.52 (s, 1H), 9.00 (s, 1H), 8.96 (s, 1H), 8.01 (d, *J* = 8.0 Hz, 1H), 7.46-7.44 (m, 1H), 7.40-7.36 (m, 1H), 7.26-7.22 (m, 1H), 7.13 (s, 1 H, 1.61 (s, 9H); ^{13}C NMR (100 MHz, $CDCl_3$, δ): 170.9, 153.3, 150.8, 138.7, 133.8, 124.8, 123.3, 120.6, 120.0, 119.7, 117.1, 115.5, 110.6, 96.0, 80.4, 28.5;

Cell cultivation

HCT-116 cell line, which was kindly provided by Prof. Bert Vogelstein (Johns Hopkins University, Howard Hughes Medical Institute, USA), was cultured in McCoy's5A medium. A-549 (CCL-185), Hep-G2 (HB-8065), U-2 OS (HTB-96), MCF-7 (HB-8065), and HEK-293 (CRL-1573) were obtained from ATCC. A-549 and MCF-7 were cultured in RPMI-1640 medium, U-2 OS in McCoy's5A medium, and HEK-293 and Hep-G2 in Dulbecco's Modified Eagle medium. The culture medium used for cancer cell lines was supplemented with 10% fetal bovine serum, 2 mM L-glutamine, and antibiotics (penicillin 62.6 µg/ml and streptomycin 40 µg/ml). Cancer cells were cultured under humidified atmosphere containing 5% CO_2 at 37°C and routinely screened for *Mycoplasma* contamination.

Cell viability assay

The cell viability was determined after treatment with the synthesized compounds using the MTT (Sigma-Aldrich) assay. Briefly, cells were seeded into 96-well culture plates and allowed to adhere overnight. Then, they were exposed to various concentrations of

compounds for 72 h. For vehicle control, DMSO (Merck) and Etoposide (Sigma-Aldrich) were used. After incubation, the MTT solution (0.4 mg/ml, final concentration) was added to the cells in each well, and the plates were incubated for an additional 2–3 h at 37°C. After incubation, the cells were stained, and the medium was replaced with 100 μl DMSO.

The absorbance of formazan was measured at 450 nm using an ASYS UVM340 microplate reader (Biochrom Ltd.). The IC_{50} value was estimated for each compound in GraphPad Prism 8 software based on the curves plotted using survival as a function of dose, averaged from three independent experiments.

Flow cytometry

For flow cytometric experiments, HCT-116, A-549, and U-2 OS cells were seeded into Petri dishes and allowed to attach overnight. Then, they were incubated with each of the investigated compounds for the appropriate time. Analysis was performed using a Guava easyCyte 8 cell sorter (Merck Millipore) and FlowJo v10 software. Each experiment was repeated independently three times.

Cell cycle analysis

For analyzing the cell cycle, the harvested cells were fixed in ice-cold 75% ethanol and stored overnight at −20°C. Then, they were rehydrated with phosphate-buffered saline (PBS) for 10 min. Subsequently, the cells were stained with 20 μg/μl propidium iodide (Sigma-Aldrich) and 50 μg/μl RNaseA (Thermo-Fisher) in PBS for 30 min at room temperature and measured.

H2AX phosphorylation

After treatment with the studied compounds, the cells were harvested and fixed in 75% ethanol overnight or longer at −20°C. To detect H2AX phosphorylation, the cells were rehydrated with PBS in ice for 10 min and permeabilized in 0.2% Triton X-100 in PBS for 5 min at room temperature. Then, they were washed with 1% bovine serum albumin (BSA) in PBS and incubated with Alexa Fluor™ 488-conjugated mouse anti-γH2AX (Ser139) antibody

(#613406, 1:100 dilution; BioLegend). DNA was stained with 20 μg/μl propidium iodide and 50 μg/μl RNaseA in PBS for 30 min at room temperature and measured.

Mitochondrial membrane potential

For determining the mitochondrial membrane potential, 10 μM Carbonyl cyanide-p-trifluoromethoxyphenylhydrazone FCCP (Sigma-Aldrich) was added 30 min before the end of incubation of cells with the investigated drug. The positive control consisted of 10 μM FCCP. After treatment, the culture medium of the HCT-116 and U-2 OS cells was replaced by a fresh medium supplemented with 5 μg/ml JC--1 dye (Sigma-Aldrich) and the cells were incubated in dark for 20 min at 37°C. Subsequently, the cells were washed twice with PBS and measured.

Reactive oxygen species generation

For analyzing the ROS generation, 1 μM CM-H_2DCFDA (#C6827; Thermo-Fisher) probe was added to the cells in each plate 30 min before the end of the drug treatment. As a reference, 250 μM H_2O_2 was used. After treatment, the cells were detached with 0.05% trypsin solution in PBS and Hank's Balanced Salt Solution, treated with 7-AAD (Sigma-Aldrich), and measured.

Apoptosis and caspase 3/7 assay

As a positive control Cells were harvested and stained with Annexin V-FITC or Alexa Fluor 488 conjugate (#A13201; Thermo-Fisher) for performing apoptosis assay or with the reagents in the CellEvent™ Caspase-3/7 Green Flow Cytometry Assay Kit (Thermo-Fisher, #C10427) for investigating the activation of caspase-3/7, according to the manufacturer's protocol. Finally, they were stained with 7-AAD (Sigma-Aldrich) and measured. For positive control, 10 μM Etoposide was used.

Senescence

After harvesting, the size and granularity of unstained cells were evaluated by analyzing the side scattering and forward scattering. Doxorubicin (Sigma-Aldrich) was used as a reference compound for the analysis.

Colony formation assay

HCT-116 and U-2 OS cell lines were seeded into six-well plates at a density of 500 cells well^{-1}. After attachment, the cells were pretreated with DMSO or different concentrations of **8** and **5aa** for 24 h. Then, they were washed and cultured for an additional 9 days. Finally, the cell colonies were fixed in methanol and stained with 0.5% crystal violet. The visible colonies were counted by ImageJ software, and percentage viability was calculated in comparison to the control.

Wound healing migration assay

The possible antimigratory effects of the tested compounds were investigated by wound healing assay. HCT-116 and U-2 OS cell lines were seeded into an Ibidi-silicone insert on a cover glass-bottom 24-well plate for live-cell imaging and incubated for 24 h to allow the attachment of cells. After incubation, the inserts were dislodged and the cells were washed twice with a fresh medium to remove any unattached cells. Then, the cells were exposed to various concentrations of compounds, and the plates containing cells were placed inside an imaging chamber (cellVivo incubation system; Olympus) maintained at 37°C with 5% CO_2 for incubation. Live-cell microscopy with time-lapse photography was performed to monitor the migration of cells. Images were captured every 15 min for 48 h under ×10 magnification using a phase-contrast fluorescence microscope (IX83 Inverted Microscope; Olympus) which was connected to an XC50 digital color camera (Olympus). Using cellSens software (Olympus), the images were combined to generate a video. The distance between gaps was measured using ImageJ software.

Immunofluorescence

Cells were treated with **5aa** and **8** at their respective IC_{50} concentrations or with DMSO (1%) or Etoposide for 24, 48, and 72 h. After treatment, they were fixed with 4% Paraformaldehyde (Sigma-Aldrich) for 15 min, permeabilized with 0.2% Triton X-100 for 15 min, and blocked with 3% BSA in PBS with 0.1% Triton X-100 (PBS-T) for 1 h at room temperature. Then, the cells were incubated with Alexa Fluor 488 mouse anti-H2AX (pS139) (#560445, 1:200 dilution; BD Pharmingen) and anti-β-Tubulin (#T8328; Sigma-Aldrich) antibodies diluted in PBS-T with 3% BSA in a humified chamber at 37°C for 1.5 h. Next, they were incubated with Alexa Fluor 594-conjugated antirabbit IgG (#sc-516250, 1:1000 dilution; Santa Cruz Biotechnology) for 1 h in a humidified chamber at 37°C. Thereafter, the cells were stained with 1 µg/ml DAPI for 10 min. Images were acquired with an LSM 800 inverted laser-scanning confocal microscope (Carl Zeiss), equipped with an airyscan detector for high-resolution confocal scanning using a ×63 1.4 NA Plan Apochromat objective (Carl Zeiss).

Confocal live-cell imaging

For the analysis of mitochondrial morphology, HCT-116 cells were grown on a cover glass-bottom confocal 12-well plate. After 6 h of treatment with the tested compounds at their IC_{50} concentration and with DMSO, mitochondria were labeled by incubating the cells with MitoTracker Green FM probe (Thermo-Fisher) and Hoechst 33342 (Thermo-Fisher) for 15 min, according to the manufacturer's protocol. After incubation, the medium was replaced with a fresh growth medium. Confocal Z-stack images were acquired at 0.5-µm intervals for 10 stacks, with the parameters (laser intensity, exposure times, gain settings, etc.) kept constant for both cells treated with compounds and cells treated with DMSO. The excitation wavelengths for MitoTracker Green FM and Hoechst 33342 were 488 and 350 nm, respectively.

Colocalization study was carried out the same way as the analysis of mitochondrial morphology with some modifications: (1) the cells were treated for 2 h with 10 µM of tested compounds, and (2) labeled with BODYPI (Thermo-Fisher) according to the manufacturer's

protocol. The excitation wavelengths for BODYPI and tested compounds were 580 and 345 nm, respectively. Correlations of overlapping pixel intensities were calculated using thresholded MCC and PCC from Z-stack images. The scatter plot and coefficients were analyzed using the JACop plugin for ImageJ as previously described.[49]

Images were acquired with an LSM 800 inverted laser-scanning confocal microscope (Carl Zeiss), equipped with an airyscan detector for high-resolution confocal scanning using a ×63 1.4 NA Plan Apochromat objective (Carl Zeiss). Cells were incubated in an incubation chamber maintained at 37°C with 5% CO_2 during the experiments.

Quantitative mitochondrial morphometric analyses

Morphometric analyses, counting of mitochondrial particles, and analysis of circularity were performed using the mitochondrial morphology plugin of ImageJ (NIH) developed by Dagda et al.[50] The average mitochondrial volume was measured using the Particle Analyzer plugin of ImageJ (NIH). All measurements were obtained from the Z-axis confocal stacks. The mitochondrial length was determined with a macro developed by Merrill et al.[51] All data were compiled and analyzed in GraphPad Prism 8.

Detection of SA-β-Gal

SA-β-Gal was detected using the protocol described by Dimri et al.[52] Briefly, after incubation, the cells were washed with PBS and fixed for 5 min at room temperature in 3% formaldehyde (Sigma-Aldrich). Then, they were washed three times with PBS and incubated for 12–16 h at 37°C (without CO_2) with staining solution (1 mg/ml X-gal; A&A Biotechnology) in 40 mM citric acid/sodium phosphate (pH 6.0; Sigma-Aldrich), 5 mM potassium ferrocyanide (Fisher Scientific), 5 mM potassium ferricyanide (Fisher Scientific), 150 mM NaCl (POCH S.A), and 2 mM $MgCl_2$ (POCH S.A). After incubation, the cells were washed again with 40 mM citric acid/sodium phosphate (pH 4.0) and observed under a BX60 inverted microscope (Olympus). SA-β-Gal-positive cells were quantified by counting the cells

in 20 random fields of view using ImageJ software. Doxorubicin (Sigma-Aldrich) was used as a reference compound for the analysis.

Statistical analyses

Statistical analyses were performed using GraphPad Prism 8 software. Data were obtained from n=3 independent experiments and are presented as mean±SEM. Statistical significance was calculated in comparison to the vehicle using one-way analysis of variance (ANOVA) post hoc Tukey's test unless stated otherwise. A probability level of $p<0.05$ was considered to be statistically significant.

References

[1] H. J. Knolker, K. R. Reddy, *Chem. Rev.* **2002**, *102*, 4303.

[2] A. W. Shmidt, K. R. Reddy, H. J. Knolker, *Chem. Rev.* **2012**, *112*, 3193.

[3] H. Yan, T. C. Mizutani, N. Nomura, T. Takakura, Y. Kitamura, H. Miura, M. Nishizawa, M. Tatsumi, N. Yamamoto, W. Sugiura, *Antivir. Chem. Chemother.* **2005**, *16*, 363.

[4] S. D. Boggs, J. D. Cobb, K. S. Gudmundsson, L. A. Jones, R. T. Matsuoka, A. Millar, D. E. Patterson, V. Samano, M. D. Trone, S. Xie, X. Zhou, *Org. Process Res. Dev.* **2007**, *11*, 539.

[5] J. D. Ha, S. K Kang, H. G. Cheon, J. K. Choi, *Bull. Korean Chem. Soc.* **2004**, *25*, 1784.

[6] G. Romeo, L. Materia, V. Pittala, M. Modica, L. Salerno, M. Siracusa, F. Russoa, K. P. Minneman, *Bioorg. Med. Chem.* **2006**, *14*, 5211.

[7] P. Bod, K. Harsányi, F. Trischler, E. Fekecs, A. Csehi, E. Hegedis, M. Donàt, G. S. Komlósi, E. H. Sziki, US 5,478,949 26 Dec **1995**.

[8] E. Ravina, The evolution of drug discovery: from traditional medicines to modern drugs Weinheim, Wiley-VCH. **2011**.

[9] J. E. Saxton, *Nat. Prod. Rep.*, **1994**, *11*, 493.

[10] Y. Zhang, V. K. R. Tangadanchu, Y. Cheng, R-G. Yang, J-M. Lin, Ch. Zhou, *ACS Med. Chem. Lett.* **2018,** *9,* 244-249.

[11] S. Maiti, A. Bose, P. Mal, *J. Org. Chem.* **2018**, *83*, 8127–8138.

[12] A. Bal, S. Maiti, P. Mal, P. *J. Org. Chem.* **2018**, *83*, 11278–11287.

[13] C. Liu, P. Knochel, *Org. Lett.* **2005**, *7*, 2543–2546.

[14] J. H. Smitrovich, J. W. Davies, *Org. Lett.* **2004,** *6*, 533–535.

[15] A. Kuwahara, K. Nakano, K. Nozaki, *J. Org. Chem.* **2005**, *70*, 413–419.

[16] L. Wang, G. Li, Y. Liu, *Org. Lett.* **2011**, *13*, 3786–3789.

[17] S. Singh, R. Samineni, S. Pabbaraja, G. Mehta, *Org. Lett.* **2019**, *21*, 3372–3376.

[18] C. Zhu, S. Ma, *Org. Lett.* **2014**, *16*, 1542–1545.

[19] S. Chen S, Y. Li, P. Ni, B. Yang, H. Huang, G. Deng, *J. Org. Chem.* **2017**, 82, 2935–2942.

[20] S. Maiti, P. Mal, *Org. Lett.* **2017**, *19*, 2454–2457.

[21] T. Watanabe, S. Oishi, N. Fujii, H. Ohno, *J. Org. Chem.* **2009**, 74, 4720–4726.

[22] M. Szewczyk, M. Ryczkowska, S. Makowiec, *Synthesis* **2019**, *51*, 4625–4634.

[23] U. Kalathiya, M. Padariya, M. Baginski, *IEEE/ACM Trans. Comput. Biol. Bioinform*. **2014**, *11*, 1196-1207.

[24] U. Kalathiya, M. Padariya, M. Baginski, *Sci Rep* **2019**, *9***,** 8707.

[25] A. Coste, G. Karthikeyan, F. Couty, G. Evano, *Synthesis*, **2009**, *17*, 2927-2934.

[26] L. Wang, Y. Murai, T. Yoshida, M. Okamoto, K. Masuda, Y. Sakihama, Y. Hashidoko, Y. Hatanaka, M. Hashimoto, *Biosci. Biotech. Bioch.*, **2014**, *78*, 1129-1134.

[27] X. Liu, Y. Liu, G. Chai, B. Qiao, X. Zhao, Z. Jiang, *Org. Lett.,* **2018**, *20*, 6298-6301.

[28] I. Wauters, H. Goossens, E. Delbeke, K. Muylaert, B. I. Roman, K. Van Hecke, V. Van Speybroeck, C. V. Stevens, *Org. Chem.,* **2015**, *80*, 8046-8054.

[29] N. Naganna, N. Madhavan, *J. Org. Chem*., **2014**, *79*, 11549-11557.

[30] K. Satoh, A. Imura, A. Miyadera, K. Kanai, Y. Yukimto, *Chem. Pharm. Bull.* **1998**, 46, 587-590.

[31] C. Mordant, S. Reymond, H. Tone, D. Lavergne, R. Touati, B. B. Hassine, V. Ratovelomanana-Vidala, J-P. Genet, *Tetrahedron* **2007**, *63*, 6115–6123.

[32] A. D'Annibale, A. Pesce, S. Resta, C. Trogolo, *Tetrahedron*, **1997**, 53, 13129-13138.

[33] B. Attenni, A. Cerreti, A. D'Annibale, S. Resta, C. Trogolo, *Tetrahedron*, **1998**, *53*, 12029-12038.

[34] P. Punda, S. Makowiec, *New J.Chem.,* **2013**, *37*, 2254.

[35] P. Punda, M. Schielmann, S. Makowiec, *Lett. Org. Chem.*, **2017**, *14*, 337-346.

[36] R. Dubey, C. E. Stivala, H. Q. Nguyen, Y.-H. Goo, A. Paul, J. E. Carette, B. M. Trost, R. Rohatgi, *Nat. Chem. Biol.* **2020**, 16 (2), 206–213.

[37] M. Olsson, B. Zhivotovsky, *Cell Death and Differ*. **2011**,18 (9), 1441–1449.

[38] G. Y. Liou, P. Storz, *Free Radic. Res*. **2010**, 44 (5), 479–496.

[39] D. B. Zorov, M. Juhaszova, S. J. Sollott, *Physiol. Rev. Suppl*., **2014**, 94 (3), 909–950.

[40] F. Sivandzade, A. Bhalerao, L. Cucullo, L. *BIO-PROTOCOL* **2019**, 9 (1), e3128.

[41] S. W. G. Tait, D. G. Green, *Oncogene*, **2008**, 27 (50), 6452–6461.

[42] S. M. Gasser, G. Daumt, G. Schatzfj, *J. Biol. Chem*. **1982**, 257 (21), 12034-12041.

[43] Alirol, E.; Martinou, J. C. *Oncogene*, **2006**, 25, 4706–4716.

[44] A. P. Trotta, J. E. Chipuk, *Cell. Mol. Life Sci.* **2017**, 74 (11), 1999–2017.

[45] D. Arnoult, *Trends in Cell Biology* **2007**, 17 (1), 6–12.

[46] M. Bonora, A. Bononi, E. De Marchi, C. Giorgi, M. Lebiedzinska, S. Marchi, S. Patergnani, A. Rimessi, J. M. Suski, A. Wojtala, M. R. Wieckowski, G. Kroemer, L. Galluzzi, P. Pinton, *Cell Cycle*, **2013**, 12 (4), 674–683.

[47] J. S. Riley, G. Quarato, C. Cloix, J. Lopez, J. O'Prey, M. Pearson, J. Chapman, H. Sesaki, L. M. Carlin, J. F. Passos, A. Wheeler, A. Oberst, M. K. Ryan, S. W. G. Tait, *The EMBO Journal,* **2018**, 37 (17), e99238.

[48] A. Chandrasekaran, M. del P. S. Idelchik, J. A. Melendez, *Redox Biology*, **2017**, 11, 91–102.

[49] S. Bolte, F. P. Cordelières, *J. Microsc.* **2006**, 224, 213–232.

[50] R. K Dagda, S. J. Cherra, S. M. Kulich, A. Tandon, D. Park, C. T. J. Chu, *Biol. Chem.* **2009**, 284, 13843–13855.

[51] R. A. Merrill, K. H. Flippo, S. Strack, *Neuromethods*. **2017**, 123, 31–48.

[52] G. P. Dimri, X. Lee, G. Basile, M. Acosta, G. Scott, C. Roskelley, E. E. Medrano, M. Linskens, I. Rubelj, O. Pereira-Smith, M. Peacocke, J. Campisi, *Natl. Acad. Sci. U. S. A.* **1995**, 92 [20], 9363–9367.